POLITECNICO DI TORINO

DIPARTIMENTO DI INGEGNERIA MECCANICA E AEREOSPAZIALE (DIMEAS)

Master's Degree Course in Biomedical Engineering

Towards an Electromyographic Armband with dry electrodes for Hand Gesture Recognition

Supervisors
Prof. Danilo Demarchi
Ph.D. Paolo Motto Ros
M.Sc. Fabio Rossi
M.Sc. Andrea Mongardi

Candidate
Andrea Zimara

TORINO, March 2021

Abstract

Gesture recognition is a computer discipline based on mathematical algorithms for the interpretation of human gestures. In recent years, recognizing and identifying hand movements have gained a lot of interest due to the increasing of Human-Computer Interface (HCI) applications like the control of mobile apps, robotics, video games, and, in the clinical field, prosthesis and robotic limb control. Several techniques are currently available for data collection: this thesis focuses on the acquisition of the surface ElectroMyoGraphic (sEMG) signal, by applying non-invasive electrodes on the skin above the muscle of interest.

This thesis work studies the implementation of dry electrodes for sEMG acquisition, evaluating signal quality by means of the Signal-to-Noise Ratio (SNR_{dB}). An acceptance value of 10 dB has been fixed, in order to consider the signal suitable for an event-based extraction technique. In particular, the final goal is to develop an embedded low-power system for gesture recognition based on the Average Threshold Crossing (ATC) technique, which is performed by establishing a threshold above the sEMG signal at rest condition and averaging the number of over-crossings inside a fixed time window.

With the aim to replace wet with dry electrodes, a first analysis involves three types of dry ones. Dry electrodes with the highest SNR_{dB} are selected for the subsequent EMG acquisitions. The sEMG signals are detected using a custom PCB developed by the research group and they are digitalized by means of a Data Acquisition System (DAQ) for further processing. To increase the SNR_{dB} a Driven Right Leg (DRL) circuit available onboard was tested in order to reduce the common-mode noise on the skin and match the body's reference potential to the circuit's reference voltage.
To allow an embedded application, the research group has developed an improved PCB characterized by a MicroController Unit (MCU) onboard. The MCU permits to transfer data via Bluetooth, so there is an incrementation of SNR_{dB} because the board's connections reduce the noise previously introduced through the DAQ system. This configuration was tested by means of procedures similar to the ones of the previous version, adding a comparison with wet electrodes.

Finally, a 3D model of the armband has been designed, composed of seven acquisition channels secured together by a plastic strip. One package was effectively prototyped to perform the tests. The SNR_{dB} calculated averaging all the contraction was equal to ~22 dB for the acquisition with wet electrodes and to ~17 dB for dry ones. The obtained SNR revealed a good quality of the acquired sEMG signal, thus confirming the feasibility of an armband for ATC-based hand gesture recognition.

Contents

List of Figures

List of Tables

Chapter 1

Introduction

1.1 Fundamentals of Muscular system

The muscular system is an organ system responsible for body movements, maintaining posture, protecting the underlying organs, and blood flow through the body. Together with the skeletal system constitutes the locomotor apparatus.
To do their job properly, the muscles must be able to respond faithfully and quickly to the commands that come from the *Central Nervous System* (CNS).
In the human body, there are about 600 different muscles that can be divided into 3 main groups [1], as shown in Figure 1.1:

- **Skeletal Muscle**: characterized by the presence of streaks and responsible for joint movements. It is controlled by the peripheral portion of the CNS, thus being a volontary muscle. Skeletal muscles are connected to the bones through tendons.
- **Cardiac Muscle**: similar to skeletal muscle because of its striation, but it is an involuntary muscle. It is located inside the heart and its contractions are due to the generation of action potentials by pacemaker cells that allow the entire network of cells to contract evenly.
- **Smooth Muscle**: its name is due to a lack of streaks, typical of previously defined muscles, thus it appears uniform, under the microscope. It is found in blood vessels, internal organs, and structures that are not under voluntary control, being activated by the autonomic nervous system.

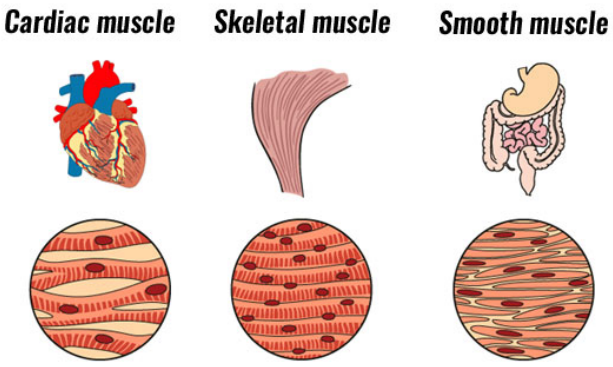

Figure 1.1: Types of muscular system [2].

1.1.1 The Skeletal Muscle

Skeletal muscles characterize the forearm, so, to efficiently develop an armband for hand gestures recognition, it becomes important to analyze the structure and functioning of this type of muscle. It is also important to analyze its operation to understand how it performs its movements, since they will be analyzed thanks to the acquiring of electromyography signal, which will be explained in Section 1.2.
Most skeletal muscles are connected to at least two bones, although there are exceptions where these are directly connected to the skin, cartilage, or other muscles. They connect to the bones through the tendons, structures formed by elastic connective tissue that transmits to the bone the muscle's strength.
Analyzing its structure, skeletal muscle consists of tissues such as skeletal muscle fibers, nerve fibers, blood vessels and connective tissue, the different sections of his structure are represented in Figure 1.2. In particular, the connective tissue consists of 3 layers, *epimysium, perimysium* and *endomysium*, which have the task of defining and maintaining the structure of the muscle [3].
The *Epymisium* is the outer layer and it has the task of protecting the muscle from friction with adjacent muscles and bones; it also allows contraction and movement. At his end, it joins with other connective tissues to form the tendons. Looking at the cross-section of the muscle it is possible to notice that the latter is structured in bundles called fascicles that are coated with the intermediate connective tissue, *Perymisium*. Inside each fascicle, there are hundreds of muscle cells named muscle fibers. The muscle fibers are equipped with different nuclei and extend along the entire length of the muscle. Each of them is coated with *Endomysium* which plays the role of transferring the force produced by the fibers themselves to the tendons. Inside, it contains the extracellular liquid and all the nutrients necessary for the fiber's survival.

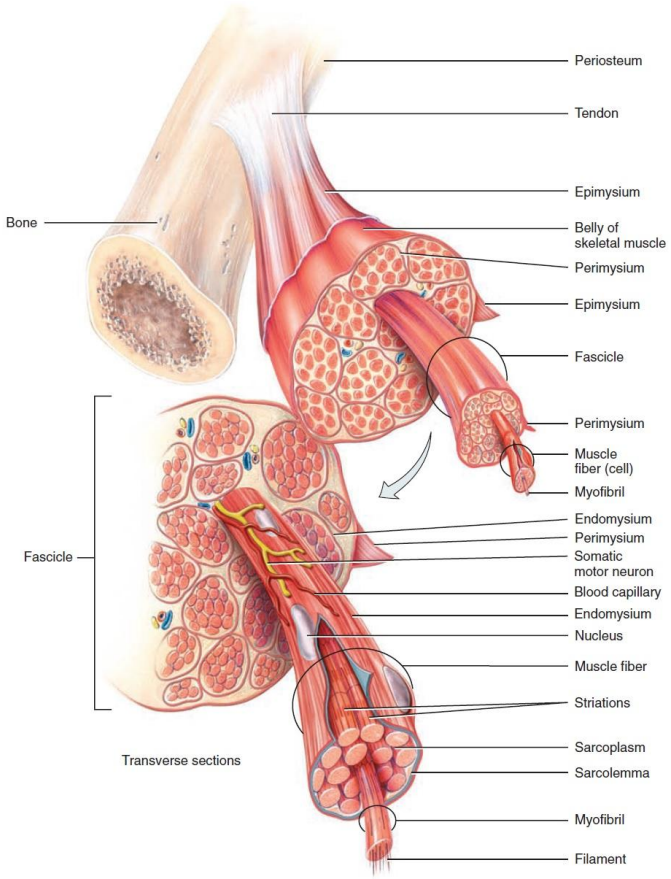

Figure 1.2: Structure of the Skeletal muscle [4].

Muscle fibers are equipped with numerous nuclei arranged below the fiber's plasma membrane, which is called *sarcolemma*. Inside the muscle fiber, there is a cytoplasm that, together with mitochondria and rod shape elements, forms structures called *myofibrils*. Myofibrils contain the contractile apparatus of muscle fiber, which consists of overlapping thick filaments formed by the myosin protein and thin filaments formed by the actin protein. Each myofibril is coated with the *sarcoplasmic reticulum* (SR) and it is in association with transverse tubules (*T tubules*), which are connected to the sarcolemma and penetrate into the cell. The sarcoplasmic reticulum has the task of storing and releasing calcium ions (Ca^{2+}) when the muscle cell is stimulated to contract. Calcium ions play the role of chemical messengers inside the cell at the level of myofibrils. They were released in response to an electrical signal and transmitted from the sarcolemma to the T tubules. As a result, SR and T tubules are very important in activating muscle contraction because, by transmitting the signal from the sarcolemma to myofibrils, they enable the cell to respond to the nervous signals.
Looking at the structure of skeletal muscle at the molecular level, muscle cells have

streaks due to the ordered arrangement of fibers within myofibrils. Along the longitudinal direction of the muscle, thick filaments and thin filaments alternate in a 2:1 ratio. The contractile unit of striated muscle tissue is the *sarcomere*; as a result, myofibrils consist of the sequence of sarcomeres.
At this point, looking at Figure 1.3, it is possible to define the **Z line**, that represents a transverse line to the longitudinal direction of the muscle and that marks the line of separation between two sarcomeres, and the **M line**, always transverse, which represents the connection between two thick filaments. At the microscopic level, in addition to these vertical lines, it's possible to observe 3 zones. The **A band**, dark, which is composed of overlapping actin and myosin filaments. **H Zone**, a small area in the middle of the A band, appears clearer, consisting only of myosin filaments. Finally, the light-colored **I Band** is composed of actin filaments [5].

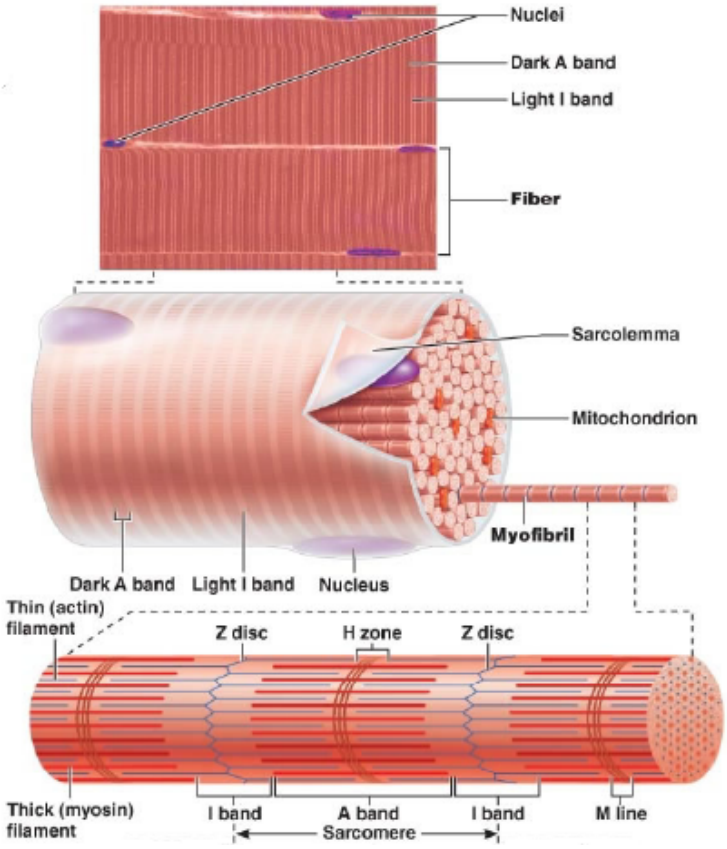

Figure 1.3: Muscle fiber [6].

The thick and thin filaments of the sarcomere, as mentioned above, are composed of **myosin** and **actin** which are contractile proteins. In particular, as can be seen in Figure 1.4, thin filaments are composed of two spiral-wrapped actin protein chains, while thick filaments are composed of myosin bands, ended by a

particular structure, named head. This head of the myosin has a dual function, it attaches to actin filaments allowing the shortening of the sarcomere and it acts as an enzyme, splitting *Adenosine TriPhosphate* into *Adenosine DiPhosphate* plus *Inorganic Phosphate*:

$$ATP \Rightarrow ADP + P_i$$

This last function is important because the execution of a contraction by the muscle requires some energy. Specifically, A bands don't change their length during a contraction while I bands and H zones become shorter. That means when the muscle cell contracts, the thick filaments don't change the length and the thin filaments flow along the thick filaments moving towards the inner part of the H zone. So, the Z lines on the sides of the sarcomere both move closer together, resulting in the shortening of the sarcomere itself. This is called model of the flow of muscle contraction filaments, and the sliding of thick and thin filaments takes the name of transverse bridge cycle.

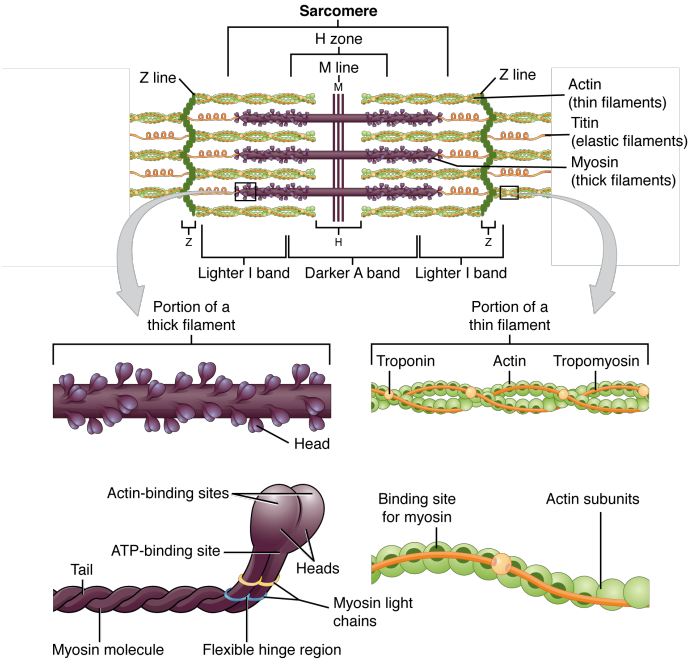

Figure 1.4: The sarcomere [3].

To perform a voluntary movement, the skeletal muscle is controlled by the peripheral part of the CNS, particularly by the *Somatic Nervous System*. The *Somatic Nervous System* has the task of transferring movements and sensory information from the CNS to the rest of the body and vice versa. In particular, the CNS is connected to skeletal muscle fibers via a single *motor neuron*. Simultaneously, however, a single motor neuron innervates several muscle fibers, the set formed by the motor neuron and all the all the muscle fibers innervated by it, takes the name of

motor unit (MU).
The MU is the functional unit of the skeletal muscle system because it is the smallest unit that can be isolated from the CNS. Observing the motor unit in more detail, looking at Figure 1.5, it is composed of 4 fundamental components:

- the *cell body*, containing the dendrites which collect the electrical signal;
- the *axon*, through which the signal is transferred;
- the *neuromuscular junction*, the point where the axon fits on the muscle fibers;
- the *muscle fibers* innervated by the motor neuron.

When an electrical impulse activates a motor neuron, this stimulates the contraction of its motor unit's muscle fibers.
Inside the muscle, however, there are several types of muscle fibers: **type I fibers**, which require oxygen consumption and are resistant to fatigue, and **type II fibers**, which do not require oxygen consumption and are less resistant to fatigue. Also, the smaller fibers are generally type I fibers, while the largest fibers are type II fibers. When a voluntary muscle contraction is performed, the CNS will not recruit motor units randomly but will recruit them according to the Henneman Principle, which says that the CNS recruits motor units from the smallest to the largest one. As a result, the smaller fibers are type I ones because they will be recruited earlier and will have to work for longer than larger type II fibers [5].

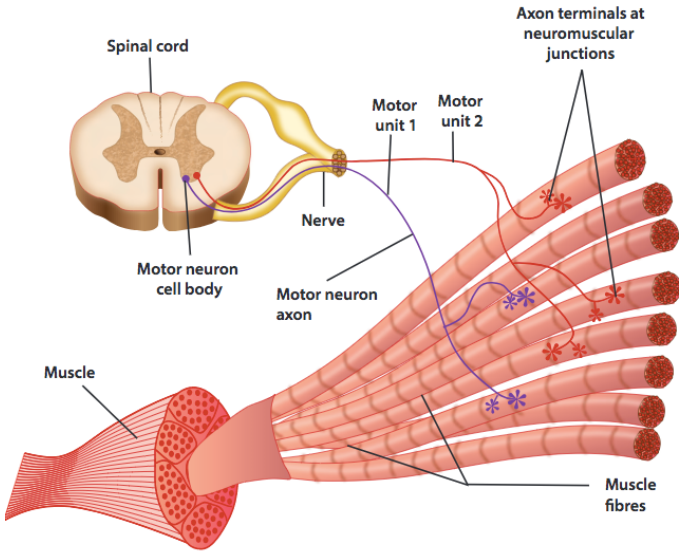

Figure 1.5: Motor unit [7]. Axon of motor neurons extend from the spinal cord to the muscle. There wach axon divides into a number of axon terminals that form neuromuscular junctions with muscle fibers scattered throughout the muscle.

Once the functioning of skeletal musle is understood, an additional distinction according to its anatomical arrangement can be made [8]. As can be seen in Figure 1.6 there are 4 different types of skeletal muscles:

- **Parallel muscles**: They are composed of parallel bundles and represent the largest group among skeletal muscles. Normally they are long muscles; as a result, their contraction causes great movements. They are not very strong, but they have good resistance. This group includes both fusiform muscles characterized by a variable diameter along its length and non-fusiform muscles that have a more rectangular shape.

- **Circular muscles**: They are composed of fibers arranged concentrically around an opening or indentation and regulate the inputs and outputs with the outside. They are typical sphincters' muscles, but they are different from the analog characterized by smooth muscles because they are under voluntary control.

- **Convergent Muscles**: These muscles are characterized by a common point of origin that is larger than the insertion point. Muscle bundles extend from the point of origin in a way that is not necessarily ordered in space, allowing to cover a large surface area. Due to his distribution, which leads to having more muscle fibers, the strength developed by these muscles is high.

- **Pennate muscles**: They are characterized by having the tendon that crosses its length. They have a large number of muscle fibers per unit; as a result, they develop very high strength, but they have the disadvantage that they get tired quickly. A further division of this group according to the fibers' arrangement concerning the tendon is possible. *Unipennate* if the bundles are on the same side of the tendon, *bipennate* if the bundles are located on both sides of the tendon, *multipennate* if the central tendon branches into the pennate muscle.

As shown in Figure 1.6, the *Extensor digitorum*, a forearm muscle, is a unipennate skeletal muscle. After giving a general view of the structure and functioning of skeletal muscles, in the next section the forearm muscles will be defined; it is really important to well define these, because the final objective of the thesis is the development of an armband for hand gestures recognition.

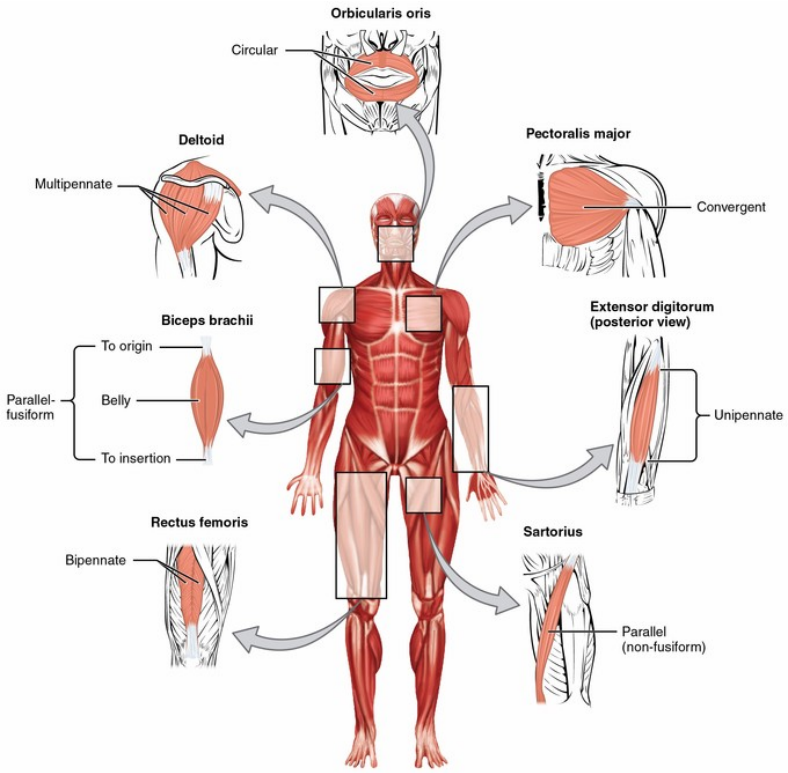

Figure 1.6: Shapes of skeletal muscle [9].

1.1.2 Forearm muscles

From a skeletal point of view, the forearm results to be quite simple as it consists of only 2 main skeletal segments: the ulna and the radio. From a muscular point of view, it becomes considerably complicated as there are different muscles to carry out the different movements. A first division is possible by separating the forearm into two compartments, an anterior compartment in which flexor muscles are present and a posterior compartment in which the extending muscles are present. In detail:

- **Anterior compartment**: the muscles in the anterior compartment of the forearm are responsible for pronation, flexion of the wrist and fingers. As shown in Figure 1.7, it's possible to make an additional division into 3 categories, superficial, intermediate and deep compartment.
  In particular, there are 4 muscles in the **superficial compartment** that have the characteristic of having the origin from a common tendon that arises from the medial epicondyle of the homer: *Flexor Carpi Ulnaris, Palmaris Longus and Flexor Carpi Radialis* are 3 muscles whose main action is that of flex-extension of the wrist, *Pronator Teres* is responsible for the pronation of the forearm.

In the **intermediate compartment**, there is only one muscle, *Flexor Digitorum Superficialis*, which has the function, when it is contracted, of flexing the metacarpal-phalanx joints, the interphalangeal joints and the wrist.
Finally, there are 3 muscles in the **deep compartment**. *Flexor Digitorum Profondus* is the only forearm muscle responsible for flexing the distal interphalangeal joints of the fingers, allows flexion of the wrist and, like the *Flexor Pollicis Longus*, allows the flexion of the metacarpal-phalanx joint, the main action of *Pronator Quadratus*, instead, is the forearm pronation [10].

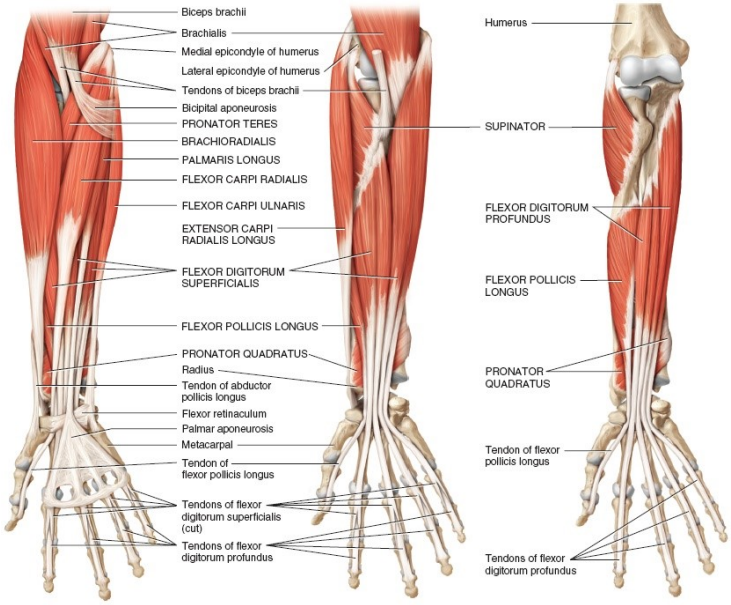

Figure 1.7: Anterior forearm muscle. From left side to right side: Superficial, Intermediate, Deep [11].

- **Posterior compartment**: the muscles in the posterior compartment are responsible for the extension of the wrist and fingers; besides, they are all innervated by the radial nerve. Similar to previous case, it is possible to further divide into 2 categories, superficial and deep compartment.
  In the **superficial compartment** there are 7 different muscles. The *Extensor Carpi Radialis Longus* and *Brevis* perform the function of wrist extension and abduction, while the *Extensor Carpi Ulnaris* of wrist extension and adduction. The *Brachioradialis* is responsible for elbow flexion; on the contrary, the *Anconeus* extends and stabilizes the elbow joint as well as abdurizing the ulna during pronation. The main action of the *Extensor Digitorum Communis* is to extend the medial 4 fingers and contributes to the extension of the wrist. The last muscle present in the surface compartment is the *Extensor Digit Minimi*

which has the task of extending the little finger and contributes to the extension of the wrist.
In the **deep compartment** there are 5 muscles. The *Supinator* who, as the name suggests, is responsible for the supination of the forearm. The *Abductor Pollicis Longus* extends and abdicates the thumb; in contrast, the *Extensor Pollicis Lungus* extends all thumb joints while the *Extensor Pollicis Brevis* extends only the prosthetic joints of the thumb. Finally, the *Extensor Indicis* has the task of extending the index finger [12].

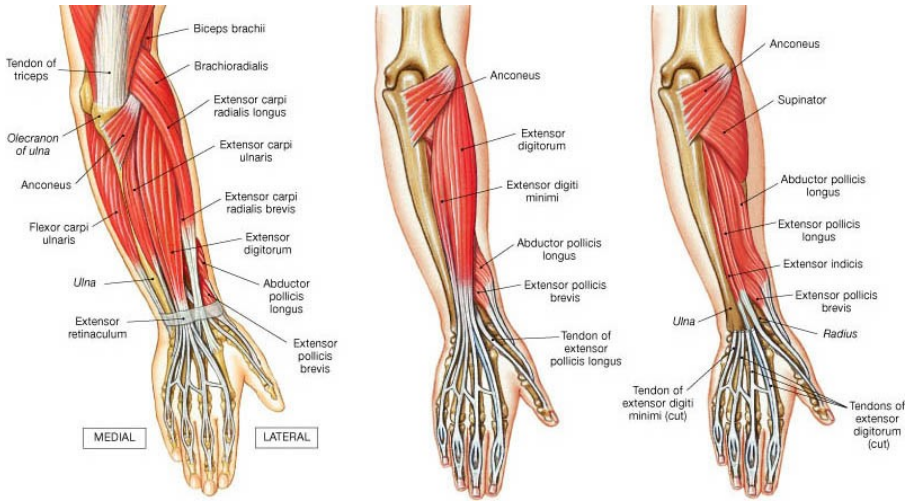

Figure 1.8: Posterior forearm muscle. From left side to right side: Superficial, Intermediate, Deep [11].

1.2 ElectroMyoGraphy (EMG)

Muscle contraction, due to the propagation of action potentials along muscle fibers, generates electrical activity, particularly an electrical signal that falls into the category of biomedical signals. With electromyography (EMG), it is possible to observe this biomedical signal. As mentioned in section 1.1.1, muscle fibers are contractile units that are controlled, not individually, by the CNS, which directly controls each MU. When a motor neuron is activated, this one will generate an action potential that propagates along the motor neuron's axon at a speed of ~70 m/s [13]. Once it arrives at the fibers innervated by the motor neuron, at the level of the neuromuscular junction, the fiber membrane will be excited with consequent generation of the *action potential of a single fiber* that propagates left and right towards the tendons with a propagation rate of about ~4 m/s [14].
The action potential is associated with a transmembrane current that determines an extracellular electric field that can be measured via EMG. In detail, the depolarization of the membrane results in the opening of the Na^+/K^+ channels resulting

in the ions moving from one part to another. The transfer of ion charges between the inside and outside of the fiber results in the generation of a single potential called **intracellular action potential (IAP)**.

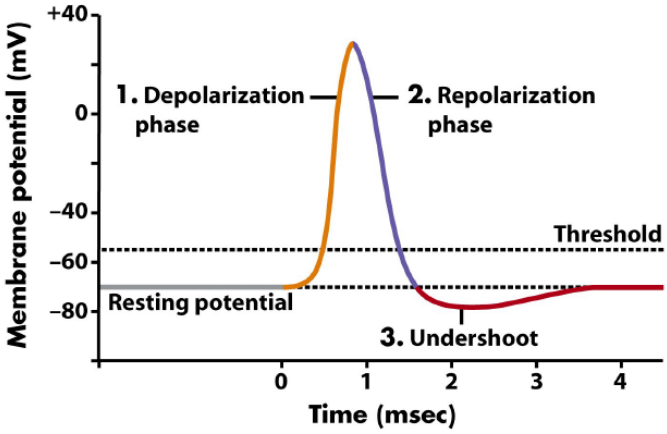

Figure 1.9: Intracellular Action Potential (IAP) [15].

As shown in Figure 1.9, IAP is divided into 3 phases: *Depolarization*, the resting membrane potential is equal to -70 mV, when it is stimulated and exceeds a certain threshold (equal to -55 mV) the action potential is generated. In the depolarization phase, there is the opening of the calcium channels with the consequent entry of the calcium ions and the peak of the membrane potential (equal to +40 mV) is reached. *Repolarization*, in which the potassium channels are opened with consequent spillage of the potassium ions; at this stage, the membrane potential descends again towards the value of the resting potential. Before stabilizing on the resting value, there is the third phase called *Hyperpolarization* in which the membrane potential becomes more negative and then stabilizes on the rest value [16]. Since the smallest command unit by the CNS is the MU, when the motor neuron is activated, an action potential is generated for each fiber innervated by the motor neuron. So, to read the signal, there will be a summation in time and space of all these action potentials and the muscle generate what is called the **motor unit action potential (MUAP)**. In addition, when a motor unit is stimulated sequentially, it generates a **train of motor unit action potentials (MUAPT)**. To acquire this electromyography signal, there are two main techniques:

- **Intramuscular EMG**: the signal acquired represents the activity of the individual motor unit, the sampling electrode is given a needle shape and it is inserted into the muscle. It is very close to the muscle, so the electrical activity doesn't have interference due to the presence of fat tissue and skin. This allows studying in detail the potential. The disadvantage of this technique is that it is an invasive technique; it can be carried out only by a doctor and cannot be used in dynamic conditions [17].

- **Surface EMG**: the signal acquired represents the activity of all motor units activated below the sampling system, the electrodes are placed externally on the skin. Consequently, this technique is non-invasive, easy to use and allows to make acquisitions in dynamic conditions [18].

In the case of surface EMG, it is possible to further distinguish biopotential sampling techniques.

Monopolar configuration: as shown in Figure 1.10, a surface electrode is placed on the skin near the muscle while a second reference electrode is placed in a neutral position. The acquired signals are the input of a differential amplifier and their difference is acquired. With this technique, the withdrawal volume is high so, even if it is easy to implement, it is not recommended as a lot of noise is acquired.

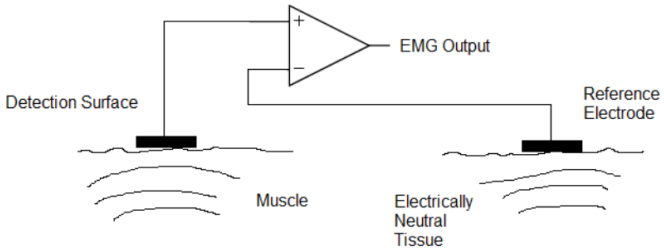

Figure 1.10: Monopolar configuration [19].

Bipolar configuration: as shown in Figure 1.11, a pair of surface electrodes is located near the muscle at an interelectrode distance of ~2 cm. In addition, there is a third reference electrode positioned in a neutral zone. The signals coming out from the two electrodes represent the input of an instrumentation amplifier that suppresses the noise common to both and amplifies the difference. This technique is called *single differential acquisition* and it is the most widely used biopotential sampling technique.

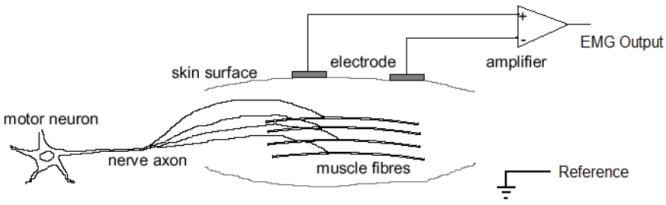

Figure 1.11: Bipolar configuration [19].

Looking at Figure 1.12, it is possible to expand the single differential acquisition by increasing the number of surface electrodes and cascading instrumentation amplifiers. If there are 3 sampling electrodes, 1 reference electrode and 3 amplifiers, that is defined as *Double differential acquisition*.

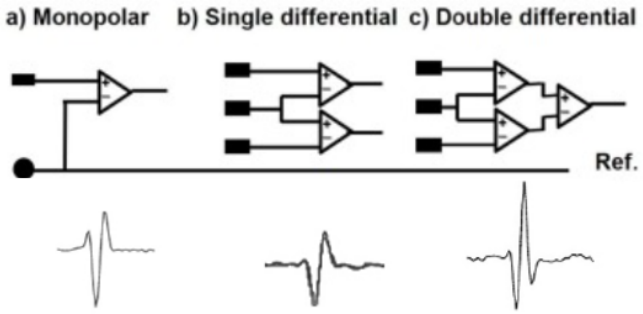

Figure 1.12: Comparison between sampling techniques, configuration and signal acquired.

1.2.1 Surface ElectroMyoGraphy (sEMG)

To perform muscle movement, the CNS must recruit several MUs to activate all the fibers of the muscle interested in movement. Through sEMG, the electromyography signal is taken, which is given by the sum of the different MUAPT that have been activated during muscle contraction. To assess the state of muscle health and the motor units recruited, it will be necessary to decompose the raw EMG signal taken as seen in Figure 1.13.

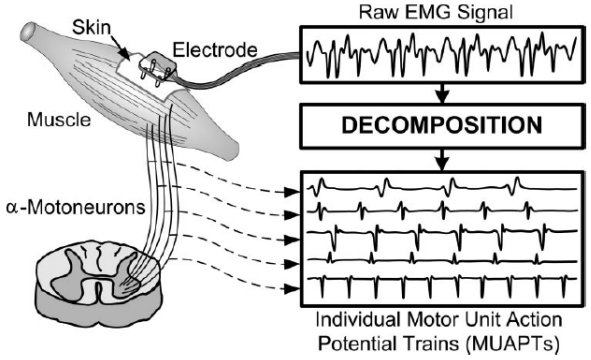

Figure 1.13: sEMG signal decomposition [20].

The sEMG technique has many applications and is mainly used for: diagnosis of neuromuscular diseases, analysis and determination of abnormalities or muscle disorders, muscle rehabilitation and using the sEMG signal for the control of prostheses and orthosis [21]. From a technical point of view, this signal has a peak-to-peak amplitude between 0 and 10 mV, while its frequency component is between 0 and 500 Hz with most information between 50-150 Hz [22].
To acquire the signal using this technique, it's necessary to place the electrodes on the subject's skin. It's possible to use a single pair of electrodes or an electrode

matrix; this depends on the final application and the precision that you want to achieve in determining muscle activity. The positioning of the electrodes with respect to the muscle turns out to be a critical step in acquiring sEMG because an incorrect positioning would result in a wrong acquisition of muscle activity. As mentioned in section 1.2, this technique has the advantage of not being invasive and being able to be used by everyone, unlike the Intramuscular EMG. At the same time, it also has some limits that are important to know when you want to use it, in particular, there are different sources of noise [23]:

- **Crosstalk**: the sampling system, in addition to observing the activity of the interested muscle, also takes the activity of neighboring muscles that have been activated. In this case, the withdrawal volume of the system may include the territory of motor units of another muscle, this type of problem is always present, but it can be reduced by improving the positioning of the electrode pair, for example, by changing the orientation of the sampling system respect to the direction of the fibers or by changing the interelectrode distance to change the acquisition volume.

- **Electrical noise**: there are two main types of noise, *intrinsic noise* introduced by electronic components and noise due to *network interference*. The first is due to the presence of electronic components and it has frequency components between 0 Hz and a few thousand Hz. It cannot be completely eliminated, but what can be done to reduce it is to use quality electronic components. The second one is generated by the electromagnetic devices present in the room; it has a wide range of frequency components even if the dominant frequency is 50 Hz for EU and 60 Hz for USA. It is important to reduce it because it has an amplitude equal to 3 times the sEMG signal.

- **Movement artifact**: this problem is caused by the interface between the electrode surface and the skin and the relative movement of the cables that connect the system to the amplifier. In this case, most frequency noise is in the range 0-20 Hz and it can be reduced with proper circuit design and quality electronic components.

- **Muscular fatigue**: In a fatigue condition, the conduction speed of the muscle fibers decreases and this leads to a reduction in the average and median frequency (explained in section 1.2.2), while observing the amplitude variables the average rectified value and the RMS value (also explained in section 1.2.2) increase.

The electrodes used to capture the sEMG signal are specific electrodes for biopotential sampling. The characteristics of these electrodes will influence the acquisition system, in particular, it will be necessary to consider their shape and size, the interelectrode distance, the material of which they are made and their positioning. The

materials must be conductive so that the electrical activity of the muscle can be observed, those that are normally used are *Ag/AgCl* (silver/silver-chloride), *AgCl* (silver-chloride), *Ag* (silver) and *Au* (gold) [23]. In addition, for doing sEMG, it is common to use 2 different types of electrodes that have the same principle of operation but differ in how they are applied. In Figure 1.16 it is possible to observe the two different models of equivalent circuits related to the 2 different types.

- **Wet electrode**: it is the most used to take EMG, EEG (*ElectroEncephaloGraphy*) and ECG (*ElectroCardioGraphy*) signal sampling tests, due to an easy application and adhesion of the electrode itself on the skin. To function, it is necessary to apply an electrolytic gel on the metal surface that will come into contact with the skin; this allows better adhesion of the electrode itself and allows to lower the electrode-skin impedance. For the metal part, the most common material is Ag/AgCl. This type of electrode, however, has some disadvantages [24], first of all, to be able to adhere well to the skin, it's necessary to apply the gel, and therefore, a preliminary phase of preparation of the skin is due. If long time acquisition is necessary, the gel under the electrode is absorbed leading to an irritation of the skin and to worsening of performance because of a change in electrical characteristics like its impedance. Finally, these electrodes are not reusable, they are disposable, and they are difficult to recycle. An example of these ones is shown in Figure 1.14.

Figure 1.14: Example of wet EMG electrode on the market [25].

- **Dry electrode**: in today society, where the Internet of Things (IoT) concept is increasing, it becomes important to have continuous monitoring even in medical applications. With the idea to have wearable devices on a patient for continuous relevant data acquisition and transmission, dry electrodes [24] have been developed. These electrodes, unlike wet ones, have the advantage of being reusable; to function, they don't need to apply any type of gel. Consequently, there is no problem of preparation and irritation of the skin, and also, there are no variations of electrical parameters like its impedance. It is possible to make long-term recordings through direct contact with the skin. However, these electrodes are characterized by a high electrode-skin impedance which has to be taken into account in the manufacture of electronic circuitry. Another problem is that to function well, they must be pressed on the skin; otherwise, they risk moving during dynamic acquisition. Finally, since there is no gel,

the fixing on the skin is more complex as it needs the application of certain supports. An example of these ones is shown in Figure 1.15.

Figure 1.15: Example dry EMG electrode on the market [26].

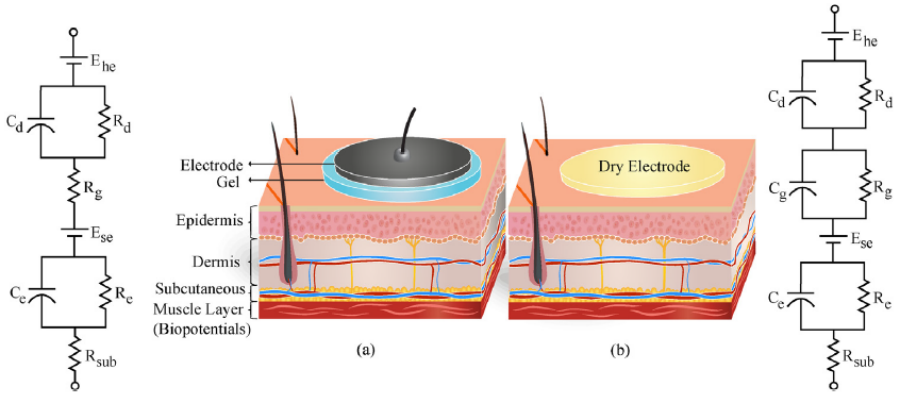

Figure 1.16: Equivalent circuit model of skin-electrode interface: a) Wet b) Dry [27].

1.2.2 sEMG features extraction

Feature extraction from sEMG is an important step for the development of a control system. As we can see in the literature, it's possible to extract the information from the signal in 2 domains: time domain and frequency domain [28].

TIME DOMAIN
The information extracted in the time domain is the most important for pattern recognition because it is easy and fast to extract. It's enough to use the amplitude of the signal, and it's not necessary to do any transformation.
Integrated EMG (IEMG): normally, it's used like a pre-activation index for muscle activity; it represents the area under the curve of the rectified EMG signal.

$$IEMG = \sum_{i=1}^{N} |x_i| \tag{1.1}$$

where N is the length of the segment, i is the increment and x_i is the amplitude.

Mean Absolute Value (MAV): it's used for detection and measurement of muscle contraction levels. It's calculated by taking the average of the absolute value of sEMG signal.

$$MAV = \frac{1}{2}\sum_{i=1}^{N}|x_i| \tag{1.2}$$

Mean Absolute Value Slope (MAVS): it represents the difference between the MAV of 2 adiacent segments.

$$MAVS_i = MAV_{i+1} - MAV_i \tag{1.3}$$

Simple Square Integral (SSI): it represents the summation of energy of EMG signal.

$$SSI = \sum_{i=1}^{N}|x_i|^2 \tag{1.4}$$

Variance of EMG (VAR): it represents the power of EMG signal as a feature.

$$VAR = \frac{1}{N-1}\sum_{i=1}^{N}x_i^2 \tag{1.5}$$

Root Mean Square (RMS): it represents the amplitude modulated Gaussian random process where RME is related to constant force and non fatiguing contractions.

$$RMS = \sqrt{\frac{1}{N}\sum_{i=1}^{N}|x_i|^2} \tag{1.6}$$

Waveform Length (WL): it's calculated like the cumulative length of the waveform over the time segment and the result represent an indicator of amplitude, frequency and duration.

$$WL = \sum_{i=1}^{N-1}|x_{i+1} - x_i| \tag{1.7}$$

FREQUENCY DOMAIN

Normally for this domain it is necessary to have more computation time because it is necessary to switch from time to frequency. Therefore, the features extracted with this method are not the best solutions for a real-time application because it is necessary to calculate the Power Spectral Density (PSD).

Frequency Median (MDF): it's based on PSD estimation and it represent the median of the PSD, it divides signal power spectrum in two areas.

$$MDF = \frac{1}{2}\sum_{i=1}^{M} PSD_i \tag{1.8}$$

where M is the length of the PSD and PSD_i is the amplitude spectrum at the i^{th} frequency .

Frequency Mean (MNF): it's also based on PSD estimation and it represent the mean value of the PSD

$$MNF = \frac{\sum_{i=1}^{M} f_i PSD_i}{\sum_{i=1}^{M} PSD_i} \tag{1.9}$$

where f_i is

$$f_i = \frac{i * SampleRate}{2M} \tag{1.10}$$

1.3 The Average Threshold Crossing (ATC) technique

To make gesture recognition, one of the possible methods is to acquire the sEMG signal and classify the made gestures through *machine learning algorithms*. The different gesture recognition systems will be presented in section 2.2. In general, data acquisition and transmission chain consist of:

- **Acquisition system**: characterized by biopotential sampling system, by applying electrodes on the skin, for example, with bipolar configuration, and which has the task of acquiring the sEMG signal.
- **Analog part**: once the raw sEMG signal is acquired, it is necessary to filter and amplify it to obtain a cleaner signal from the noise; in this part, a preprocessing is carried out.
- **Digital part**: finally, there is an A/D converter that has the task of converting the filtered sEMG signal into a digital signal. The A/D converter is, for example, controlled by a microcontroller that can have the task of analyzing the digital signal directly or transferring it to a computer.

The sEMG signal contains a lot of information, so, to consider the continuous variation of IAP, to analyze this signal, the research group have developed a technique based on the application of a threshold to reduce the data to be analyzed.
The *Average Threshold Crossing (ATC) Technique* is an event-driven technique

that leads to the creation of a quasi-digital signal. This technique is explained in detail in the following works [29], [30] and [31]. In short, a threshold is defined for each acquisition channel and each time the sEMG signal exceeds this threshold, an event called *Threshold Crossing (TC)* is raised. Next, a time window is defined to count the of TC events that have been raised, that is, it counts the number of times the sEMG signal exceeds the threshold value. This signal is defined as quasi-digital because, for its generation, an A/D converter is not used. Still, it is generated via hardware using a two-input voltage comparator. One input is represented by the threshold and the other by the filtered and amplified sEMG signal. At the output of the voltage comparator, the quasi-digital signal is then generated. In particular, there is a high level when the sEMG signal has a value greater than the threshold and a low level otherwise, so it's getting signal information over time and not in its analog value. In Figure 1.17 it is possible to observe the operation of the ATC technique and the voltage comparator.

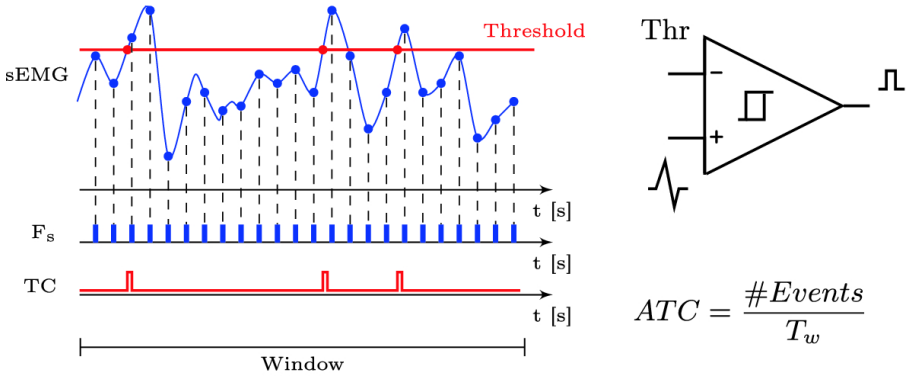

Figure 1.17: Average Threshold Crossing (ATC).

The TC signal can be used directly as an input of a microcontroller; this translates into the fact that there is no need to use an A/D converter. This is particularly important when it is wanted to develop a wearable system. First, the complexity of electronic circuitry and the area occupied by the components decrease. Moreover, this event-driven technique leads to a decrease in packets transmitted wirelessly with a consequent decrease in consumption; thus, this technique is characterized by low energy consumption. ATC technique can be used to make gesture recognition but cannot be used to make diagnoses because the sEMG signal is denatured with consequent loss of information both in time and frequency. So, it is impossible to do the reverse process that reconstructs the sEMG signal starting from the ATC signal.

1.4 Machine Learning Classification Algorithms

Machine Learning (ML), a branch of *Artificial Intelligence (AI)*, consists of learning based on data to be analyzed and, therefore, on the experience acquired in their treatment. Many times these two terms are confused, but it is necessary to separate them. Machine learning is under artificial intelligence, but artificial intelligence is not just machine learning [32]. As will be in Chapter 2, to do Gesture Recognition, different machine learning classifiers are used regardless of the various data provided as input. First, looking at Figure 1.18, classifiers can be grouped into two main groups [33]:

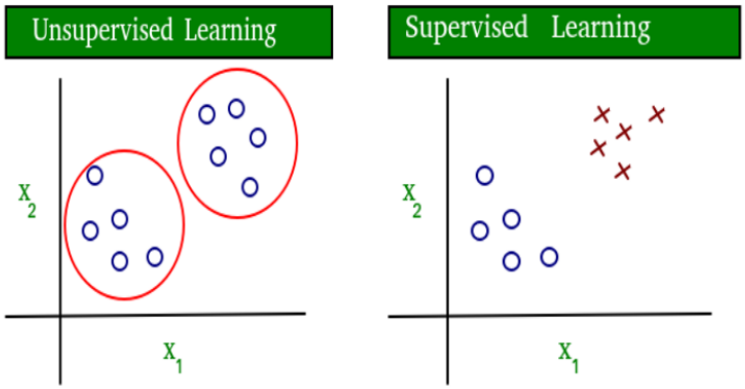

Figure 1.18: Unsupervised vs Supervised Learning Algorithms [34].

- **Unsupervised Learning**: no label needs to be associated with the classifier's incoming data. The main role of this learning is generally data clustering. Also, it's possible to do association rule learning. Some of the main algorithms in this category are *K-means* and *Gaussian Mixture Modelling*.
- **Supervised Learning**: In this case, each input data is assigned a label indicating the class to which it belongs. With this learning, it's necessary to have separate data if there is only one dataset, divided into training sets and test sets with a percentage generally of 70-80% for training and 30-20% for testing. Otherwise, if there are two datasets, one is used for training and the other for testing. The main use with this type of learning is to do classification or regression. The main algorithms in this category are *Random Forest, Support Vector Machine, Naive Bayes,* and *Neural Network*.

Moreover, two additional categories of machine learning need to be mentioned. **Semi-supervised Learning Algorithm** which is a middle ground between the two defined above. For training both data with its associated label and unlabeled data are provided. **Reinforcement learning Algorithm** makes decisions based on actions to be taken to achieve a better result. In particular, these algorithms

use estimated errors such as rewards or penalties.
A brief theoretical description of the different types of supervised and unsupervised learning mentioned above follows.

1.4.1 K-means

K-means is one of the most important machine learning algorithms used for clustering. As mentioned above, this is unsupervised learning whose data is characterized by not having label-related information. K-means is an iterative method that has the purpose of dispersing data in different clusters.

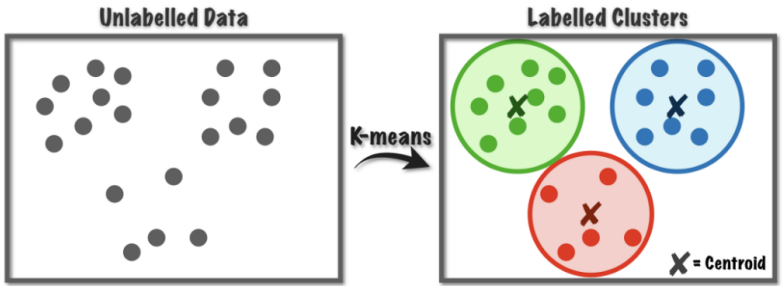

Figure 1.19: K-means clustering.

Initially, it is defined a k value that corresponds to the number of clusters in which the dataset should be divided [35], with $k = 2$, the data will be divided into two parts, with $k = 3$ in three parts and so on. For each k cluster, the centroid is calculated, for example, such as the average value of values within the cluster or a random value is chosen within the cluster. It calculates the distance between each data of the dataset with each of the k centroids at each iteration. To cluster, the data is attributed to the cluster whose distance is smaller. Also, at each iteration, it recalculates the centroid's value because there is a variation of elements inside the cluster. This method is iterative and it will end or defining a priori a fixed number of iterations, or when the change in calculating of centroid it will be stabilized. The distance between the data and the centroid can be the *Euclidean distance*, defined as:

$$d(x_i, y_i) = \sqrt{(x_i - y_i)^2} \tag{1.11}$$

Where x_i and y_i are 2 vectors.
The key parameters that are evaluated in clustering are *intra-cluster variability* and *inter-cluster distance*. The goal is to achieve low intra-cluster variability and high inter-cluster distance.
The advantages of the K-means algorithm are the easiness of implementation, the ability to adapt to large datasets, and it ensures convergence. Its disadvantages relate to the initial choice of k with its relative dependence on initial values and the difficulty in clustering outliers.

1.4.2 Gaussian Mixture Modelling (GMM)

Unsupervised algorithm used for clustering, based on a probabilistic approach. The data is organized into several Gaussian distributions, each representing a different cluster. In particular, the data will be assigned to the cluster with the highest probability of membership. Due to Gaussian distributions, each cluster is characterized by unknown parameters, such as mean and variance, which are calculated by the algorithm implementing the expectation-maximization (EM) [36]. Looking at Figure 1.20, GMM allows the implementation of different covariance types that allow to better define the different clusters: *spherical, diagonal, tied* and *full*.

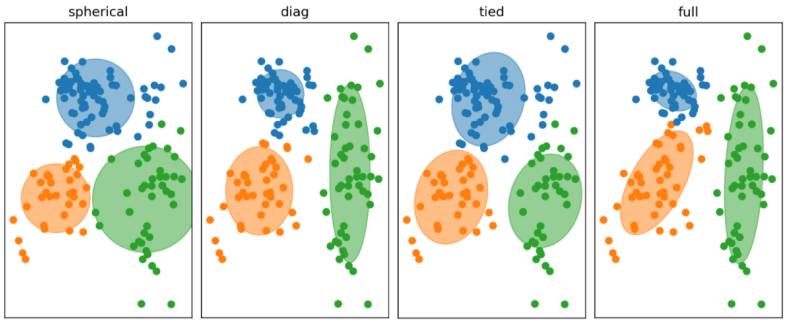

Figure 1.20: Different types of covariance.

An advantage of the GMM algorithm is that it allows to create clusters composed of a small number of data and also represents a generalization of K-means as in its evaluations, it also takes information from the data's covariance. The disadvantages are that it is difficult to estimate the correct number of clusters and, during its implementation, it has to perform many operations that lead it to have a high computational cost.

1.4.3 Random Forest (RF)

First, in order to evaluate the functioning of this algorithm, it is necessary to introduce the **Decision Tree algorithm**, a non-parametric supervised learning method used to make classification and regression [37]. This algorithm, showns in Figure 1.21 is based on decisions that form a branched structure. In particular, 3 fundamental nodes connected by branches are defined: *root node* that represents the starting decision, *decision node* that represents the various decisions to be made to converge to a class and the *leaf node* that represents the final classification of the data.

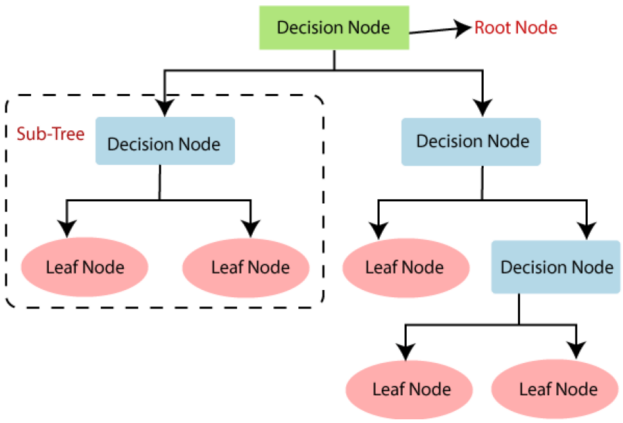

Figure 1.21: Decision tree algorithm [38].

What has been defined so far represents a single decision tree. What Random Forest does is to create a forest of classification trees that leads to a definitive choice of the class based on an evaluation of many trees. The final result represents the majority of the forecasts obtained. By evaluating many random trees, the result is more accurate than that obtained by a single decision. In Figure 1.22 is shown the Random Forest structure.

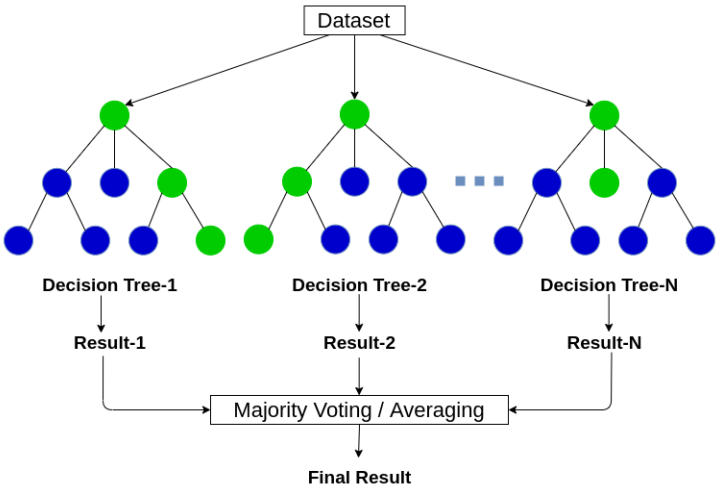

Figure 1.22: Random forest algorithm [38].

One of the main advantages of this algorithm is the reduction of the overfitting problem. Moreover, it is based on decisions, so it is not necessary to perform a normalization of the data which can have both categorical both continuous values. Considering the disadvantages, this algorithm is formed of many decision trees , thus requiring a high computational cost to obtain outputs from each of them and combine the various results.

1.4.4 Support Vector Machine (SVM)

Supervised machine learning technique used for classification and regression. SVM is based on the principle of margin calculation, in particular, it draws the margins between classes in order to obtain the maximum distance between class and margins with the objective to minimize classification error. The basic concepts of this algorithm are [39]:

- *Separating hyperplane*: Imagining to have data that can be easily separated linearly, SVM draws a line between the different clusters. In an N-size SVM space, it draws a separation to N-1 dimensions. So, in the case of 2 dimensions a row is drawn and in the case of 3 dimension a plane is drawn.
- *Maximum margin hyperplane*: SVM draws several lines to separate the clusters; each of them will lead to a different classification. SVM takes the line that is about halfway between the different clusters and has the maximum distance from the marginal components belonging to the different clusters to maximize the correct classification.

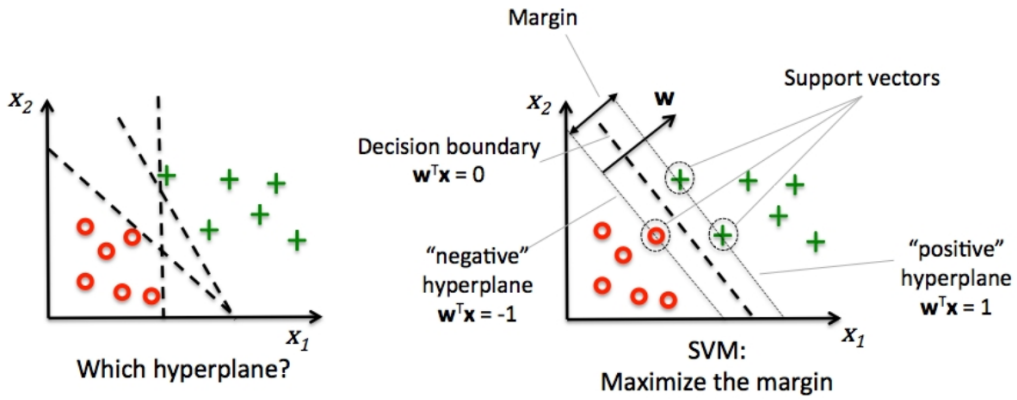

Figure 1.23: SVM hyperplane [40].

In Figure 1.23 it is possible to observe how the data is easily separable linearly; however, since it is possible to have nonlinear data available, it is important to define another parameter.

- *Kernell function*: A mathematical solution that allows the SVM to classify data by adding a dimension. In Figure 1.24, it's possible to see how the data are separate by adding a dimension. It's necessary to be careful in choosing the Kernel as adding size could lead to an exponential increase in the search for solutions as the data is characterized by an extra dimension.

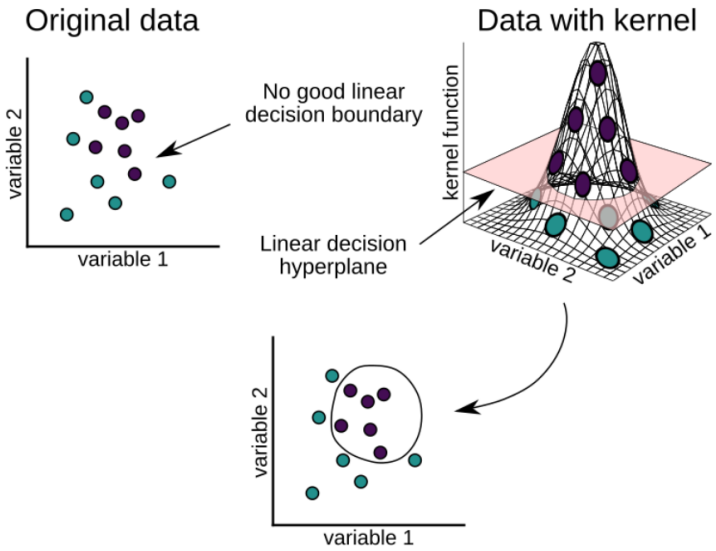

Figure 1.24: Kernel function [41].

The advantages of SVM are that it is a versatile algorithm because you can use different kernel functions, it is efficient both in terms of memory and when the number of dimensions is greater than the number of samples. Its disadvantages are operating problems when classes overlap and do not define any probabilistic classification estimation. It has problems even if the number of functions per data is greater than the number of trained sample data.

1.4.5 Naive Bayes (NB)

Supervised learning algorithm used for clustering and classification built on a probabilistic classifier. It is based on *Bayes theorem* with 2 assumptions, it considers each data as an independent value and each data give the same contribution for the result [37]. Moreover, it is defined as a probabilistic classifier because it is built on conditional probability, which means the algorithm calculates the probability of an event looking at something before, as shown in Figure 1.25. The mathematical expression of Bayes theorem is:

$$P(y|x) = \frac{P(x,y)P(y)}{P(x)} \tag{1.12}$$

Using the probability terminology the prior equation can be written as:

$$Posterior = \frac{Prior * Likelihood}{Evidence}$$

Where the Prior therm is defined as

$$P(y,x) = \prod_{j=1}^{d} P(x_j|y) \tag{1.13}$$

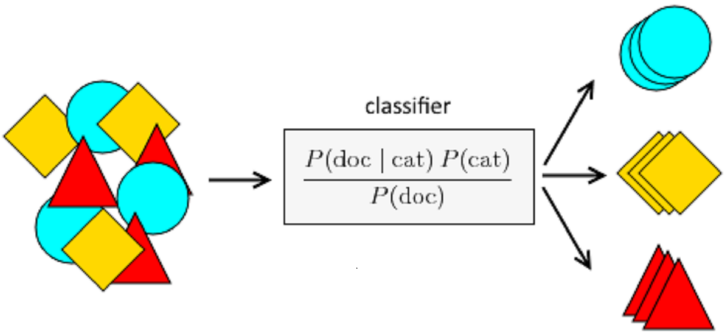

Figure 1.25: Naive Bayes classifier, an example of conditional probability with classification of dogs and cats.

This algorithm's advantages are that it has a short operating time, is suitable for solving multiclass problems and provides better performance than other classifiers when the independence hypothesis is verified. Precisely, this is one of the main disadvantages of this algorithm. In reality, it is difficult to verify the hypothesis of independence, leading to the possibility of incorrect estimates.

1.4.6 Neural Network (NN)

Neural Network, or Artificial Neural Network (ANN), is a machine learning algorithm that tries to create links to store and elaborate information like the human brain. The brain is characterized by numerous neurons that communicate with each other through synapses, in the case of NN, it is important to define some fundamental parameters to simulate brain activity. It is necessary to specify the number of neurons, define how neurons are connected to each other and define the learning algorithm. Particularly, in the case of the supervised learning algorithm, the NN will make classification and in the case of unsupervised learning algorithm NN will create clusters [37]. In the case of supervised NN, the algorithm is iterative. At each iteration in the training phase, it changes neurons' weight to decrease the classification error. Each neuron is called perceptron; the most common NN is characterized by many neurons and is called multi-layer perceptron. 3 main layers are defined as can be seen in Figure 1.26:

- *Input layer*: neurons that receive input directly from the external environment.
- *Hidden layer*: receive and analyze data from the input layer or other hidden layers. It's possible to define several hidden layers.
- *Output layer*: after the hidden layer processing information, it provides output for the external environment.

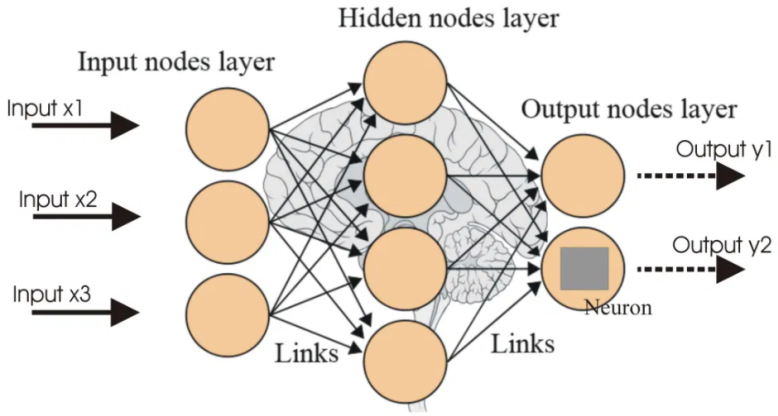

Figure 1.26: Layers of Artificial Neural Network [42].

Each neuron is formed by a certain activation function that must be satisfied in order to activate the neuron, this activation function can be linear or non-linear. The advantages of neural networks are that following training, it can process data with incomplete information, has good performance even with non-linear data and has a high computing power that allows performing multiple processing simultaneously. However, neural networks generate an output without knowing the exact obtaining procedure. For the training phase requires a high amount of data, many more than the other algorithms, which involves a high computational cost.

Chapter 2

State of the art

2.1 ATC application in sEMG detection

In the literature of recent years, it is possible to observe several studies in which the ATC technique has been used in sEMG applications. An important work in this field was carried out by the *Istituto Italiano di Tecnologia (IIT)* which demonstrated the possibility to acquire strength muscle information using the ATC technique combined with an Impulse Radio Ultra-Wide Band (IR-UWB) technology.

In the first study [43], they did was about the development of a wireless device for biomedical applications. Taking advantage of the ATC technique, they combined it with the IR-UWS wireless protocol instead; so, they don't transmit the entire sEMG signal but only short pulses. This reduces the power consumption. In particular, the data was transferred each time a TC event was generated. In this article, they also validate the ATC parameter by calculating the correlation between this parameter and the muscle strength value, acquired by the dynamometer, and between the force value and the Average Rectified Value (ARV) of the sEMG signal. They obtained a correlation between ATC and force of 0.95 ± 0.02 and a correlation between strength and ARV of 0.97 ± 0.02.
After that, a second work was done [44] starting from what was described in the previous paragraph in which some improvements were introduced. It was applied a multichannel capture and wireless data transmission took place through an Address-Event Representation (ER) approach. This study further underlined that using the ATC technique comports a reduction in power consumption. Also, there is a reduction in the board's size as thanks to the use of quasi-digital signal it is not necessary to insert the ADC inside the board. To further validate the ATC parameter, its robustness was considered by evaluating some parameters. When the signal to noise ratio (SNR) changes, certain robustness of the ATC parameter is obtained for values greater than 5-6 dB. Moreover, the latter is not affected by distortion and saturation effects of the amplifier. Finally, by assessing event losses, the correlation was maintained with a tolerance of 70% of lost events.

In [45] it is developed a wearable device to capture and process sEMG data that use the ATC event-driven approach to reduce data that would be used later in the evaluation of muscle activity patterns in rehabilitation medicine. [46] developed a wearable acquisition board on which experimental validation tests were carried out. In [30] the ATC technique has been used to develop a system that would control in real-time *Functional Electrical Stimulation (FES)*, a technique that allows functional muscle contraction through the application of a stimulator and that is applied in the rehabilitation field where support to the patient is needed to make certain movements.

Finally, in recent years, it's started to use the ATC technique to make Hand Gesture Recognition, a discipline that will be explained in Section 2.2. The first work on this topic was carried out by [47] in which, through 3 acquisition channels positioned on the forearm, it was acquired the ATC signal characteristic of 4 hand movements (*wrist flexion, wrist extension, hand grasp, wrist radial*). The acquired signal was used to train Machine Learning Algorithms that allow gesture recognition. It is used the Support Vector Machine (SVM) algorithm that was trained on MATLAB using statistics and machine learning toolbox. The classifier reported satisfactory results both in terms of accuracy and classification time. In particular, it was obtained an average accuracy of 92.87% and a latency period of 160 ms. The subsequent work on this area was carried out by [31]. It was increased the number of gestures to be classified; in addition to those mentioned above the *wrist ulnar deviation* and *idle state* gestures were introduced. Also, in this work, the classifier was uploaded to an MCU, Apollo2 of Ambiq (low-power device) to make an embedded system. In this study, a neural network (NN) was used as a classifier and with the dataset used it was obtained an average accuracy of 92.3% and latency of 268.5 ms. [48] evaluated the same dataset [31] using other classification algorithms, SVM classifier and K-Means classifier. The first case achieved an average accuracy of 94.49% with an overall latency of 239.85 ms. In contrast, in the second case, an average accuracy of 95.14% with a total latency of 130,124 ms was obtained. Lastly, in [49] the prior dataset was further expanded with two gestures (*pinch grip* and *open hand*); in total, there were a total of 8 movements. This work focused on evaluating different machine learning algorithms, in particular, it was considered NN, SVM, Random Forest (RF), Naive Bayes (NB) and Gaussian Mixture Modelling (GMM). Considering a balance between the parameters, the best performing is the NB classifier characterized by accuracy of 81.5%, a classification time of 140 µs and energy per prevision of 0.55 µJ.

2.2 Gesture recognition

Gesture recognition is a computer discipline based on the use of mathematical algorithms for the interpretation of human gestures. In recent years, recognizing and identifying hand movement have gained a lot of interest due to the increasing of Human-Computer Interface (HCI), some examples of application are reported in Figure 2.1. Regardless of their application, gesture recognition systems are made as follows:

$$\textit{Data acquisition} \Rightarrow \textit{Feature extraction} \Rightarrow \textit{Classification}$$

As shown in the literature [50], gesture recognition systems have several applications.

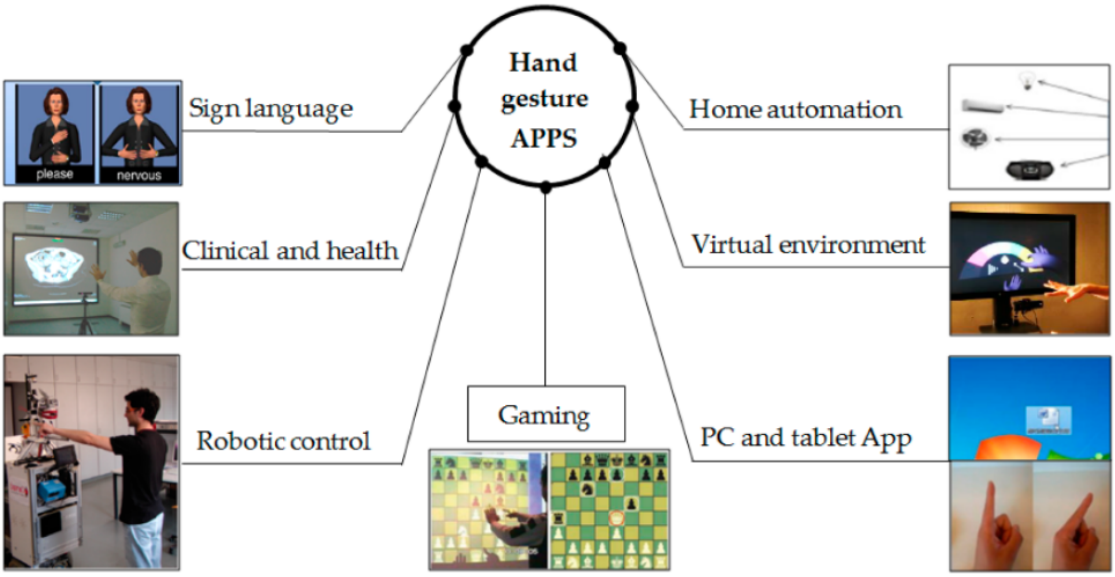

Figure 2.1: Common application area of hand gesture recognition system [51].

PC and Tablet App. Hand movements can be used as an alternative input device when interacting with PCs by creating direct interaction between the user and the desktop. For example, by using systems that recognize the gesture, it's possible to control the mouse, drag files, move and paste files and control slides in a presentation [51]. Also, considering the smart wearable devices that are becoming more and more popular, it's possible to think it's using can directly control applications. [52] has proposed a smartphone application that uses the smartwatch for gesture recognition, these devices are connected via Bluetooth. In particular, inside the smartwatch, there are some sensors such as an accelerometer, linear accelerometer and gyroscope; thanks to that, it is possible to identify the movement of the user's wrist. In this work, it is possible to download an application on Smartphone

and Smartwatch that captures the data provided by the sensors and classifies in real-time the gestures made using Tensorflow. The frequency of data acquisition from sensors is 100 Hz. Those are classified 5 different movements with a Bidirectional LSTM based deep neural network model, it is obtained an accuracy of 96%.

Virtual Environment. This is based on a 3D model. Thanks to hand gesture recognition, it is possible to interact in real-time with the model and manipulate virtual objects [51].

Home Automation. With the development of home automation, intending to have a home characterized by many smart appliances, it is possible to think of using gesture recognition to control smart devices. [53] proposed the use of a smartwatch containing different sensors (accelerometers and gyroscopes) for the control of household appliances inside a house, taking advantage of the movements of the hand. The proposed system consists of 3 parts, the smartwatch for data acquisition and transmission, the smartphone on which there is an application that has the task of classifying the gesture made and sending the data to the home automation platform, and finally, the home automation platform with its connected smart devices. From 20 different subjects are asked to perform 18 different gestures to classify. The sampling frequency of the smartwatch is 25 Hz. Two different neural networks have been implemented to perform gesture recognition, based on a deep convolutional neural network (CNN) and a DeepConvLSTM. To assess the accuracy in the classification, F-1 Score was calculated, for CNN a value of 73.7% was obtained, while in the case of DeepConvLSTM a value of 75.8%.

Robotic control. It's considered one of the most interesting applications. An example is a human-robot interaction proposed by B. MA et al. [54] in which the acquisition of images via Kinect camera is controlled by a hexagonal robot. They developed a system that detects fingertips. In particular, it continuously captures the image of the fingertips from which it creates a hand model, compares the model with a library containing the hand gestures and once it is located, it wirelessly transfers the information to the robot that will change its shape (hexagon, square, triangle, etc.).

Gaming. The purpose of this application is to allow greater physical interaction by the user with virtual reality. In the article proposed by S. Rautaray and A. Agrawal [55], it was used some image processing algorithms such as Camshift and Lucas Kanade along with haar cascade classifier in which the acceptability, usefulness and ease of use by the user have been taken into account to demonstrate the accuracy of the system. The application must meet the constraints of classifying the gesture in real-time. Image processing techniques have been implemented in C++ using the OpenCV library. In this game, the user makes 4 gesture to move

a man attacked by a bird. 15 different users were considered t assess performance. The results show a gesture recognition rate from 93% to 80% for different gestures.

Sign language recognition. This kind of application would make it possible to overcome communication barriers by deaf people with the rest of society. Ming Jin Cheok et al. [56] propose in detail analysis of the techniques used in hand gesture recognition; in particular, sign language. It is also remembered that the fundamental parameters in the evaluation of this kind of system are scalability, robustness, user independence and real-time application. Sign language is particularly complex in that it includes movements of fingers, hands, arms, head, body and facial expressions, and there are different types of language. The most widely used in literature are the American Sign Language (ASL), Indian (ISL) and Arabic (ArSL). An analysis of the different gesture recognition techniques is carried out, both through the use of cameras both through sensors and different types of classifiers (SVM, ANN, k-NN, unsupervised static classification method) are compared. In this article, some tables contain interesting results. In the case of vision-based gesture recognition, evaluating the accuracy in classifying the ASL, accuracy values are obtained between 89.1% and 95% using HMM classifier. In the case of sensor-based gesture recognition, evaluating the accuracy in classifying the ASL, the results are from 79.83% with SVM classifier to 99.1% using MLP-NN Naive Bayes classifier.

Clinical and health. With greater human-machine interaction, it's possible to use gesture recognition to control prostheses and orthosis and manipulate digital images by a doctor during an operation while keeping your hands sterile. J. P. Wachs et al. [57] proposed a system called "*Gestix*", video capture and hand gesture recognition system used for handling and navigating MRI images within a medical record. The system had a frame rate of 150 Hz and was tested by a surgeon during 2 neurosurgical biopsy surgeries at Washington Hospital Center. Subsequently, tests were carried out by 10 students who reported accuracy of gesture recognition equal to 96% for the 8 gestures made.

Looking before, it's possible to see that there are different types of systems to be able to do hand gesture recognition that is based on different data acquisition systems:

- **Stereo camera**: Mohidul Alam Laskar et al. [58] have proposed a method for hand gesture recognition based on stereo cameras. They wanted to go from 2D recognition to 3D recognition so they could also take advantage of depth information. Before capturing the images to be classified, there was a preliminary calibration of 2 RGB sensorsand grinding phase of the cameras in which the geometric relationship between them was calculated. Next, images captured from both cameras are match and produce a disparity map on which

the features (position, orientation, and speed) that will be sent to the classifier are extracted. In this case, the classifier used was Conditional Random Field (CRF). The software was implemented using the OpenCV 2.0 library on C/C++ programming. The results show an average recognition rate of 88% for the classification of Arabic numbers (0-9).

- **Motion capture**: motion capture systems can be used to perform hand gesture recognition. In the article written by N. Bargellesi et al. [59] an algorithm for gestural recognition of hand movements has been proposed. The motion capture proposed system consisted of 12 infrared cameras capturing three-dimensional position data of 8 markers, and the cameras have a sampling frequency of 340 Hz. Like all MoCAP systems, it is initially necessary to perform a phase of identification of markers during camera calibration, the paper specifies how the coordinate reference system was placed in the center of the room in the direction of the completion of the gestures. Three different methods of extracting features were evaluated, they were passed to a recognition algorithm. In this case, it was the Random Forest classifier. The three different feature extraction techniques were time-series cropping (CROP), time series resampling (RESAMP) and summary statistics (STAT). The results show gesture accuracy values of 93% for CROP, 97% for RESAMP and 96% for STAT.

- **Wired gloves**: T. Chouhan et al. [60] have developed a low-cost wired glove to recognize hand and finger orientation with 7 bending sensors, 4 Hall effect sensors, and one 3-axis accelerometer. The data captured by the different sensors is temporarily stored in an array. Then they are transmitted sequentially to a computer via a Universal Asynchronous Reception and Transmission (UART) connection. In the first phase, the data arriving on PC is processed by a MATLAB script that has the task of training the supervised learning algorithm (logistic regression), in the second phase, the data that arrives on the PC are classified by the trained algorithm. For each patient, it was asked to repeat 20 times each of the 10 gestures they wanted to classify. The results obtained show that an average accuracy of 96% has been achieved.

- **sEMG signal**: the sEMG, as described in section 1.2, has many applications. S. Benatti et al. [61] has developed a wearable device based on sEMG for real-time hand gesture recognition, an example of the chain of gesture recognition based on sEMG is shown in Figure 2.2. The system developed consists of Cerebro Afe multichannel that interfaces via SPI to an ARM Cortex M4 microcontroller which has the task of acquiring data and performing classification. The data can be stored on an SD card or transmitted via Bluetooth to a host device. As a recognition algorithm, SVM Classifier was used. In an initial phase of training the acquired data was transmitted via Bluetooth

on PC and offline SVM training took place through a MATLAB script. Once trained, the SVM was loaded into the microcontroller to perform a real-time classification. The acquisition system consisted of 8 channels and a sampling frequency of 1 kHz, the dataset was composed of 4 healthy subjects who were asked to perform 7 movements to be classified. An average accuracy of 89.2% (92% maximum) was obtained with a computational time satisfactory for a real-time application.

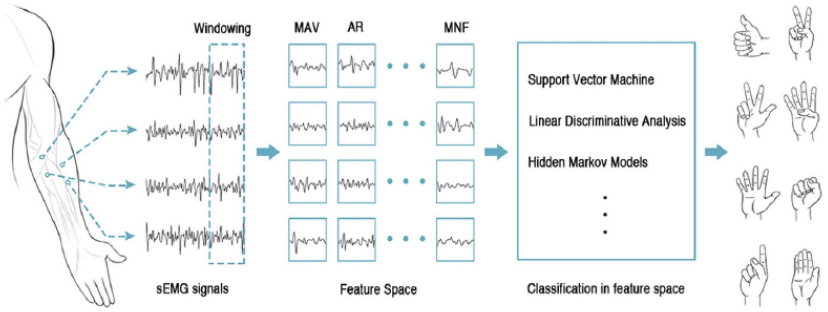

Figure 2.2: Chain of sEMG gesture recognition based on feature extraction [62].

2.3 EMG Armband for hand gesture recognition

2.3.1 gForce-Pro EMG Armband by Oymotion

Oymotion is a start-up founded in 2015 in Shanghai, that deals with the development of biometric sensors, artificial intelligence algorithms to interpret biomedical signals and gesture control based on EMG, intelligent orthosis and intelligent prosthetic hand [63]. They have developed a gesture recognition armband, gForce-Pro, which monitors biometric forearm signals to track arm position. It's possible to see the gForce-Pro Armband in Figure 2.3.

Figure 2.3: gForce Gesture Armband [63].

gForce-Pro allows the recognition of 8 gestures; from a technical point of view,

this band consists of 8 acquisition channels with bipolar configuration (dry electrode) and a 9-axis motion sensor (accelerometer, gyroscope, magnetometer). The acquired data is transferred via Bluetooth (BLE4.2) at a maximum distance of 10 meters and the supported platforms with which gForce-Pro can interact are Windows, Android, or MCU like Arduino. The maximum sampling frequency is 1000 Hz, and via hardware, a band-pass filter is applied between 20-500 Hz with a gain of 1000. Conversion to digital signal is done using an A/D converter. The microcontroller present in this device is an ARM Cortex M4 High Performance and the armband is characterized by low power consumption (below 0.1 W).

2.3.2 Myo Armband by Thalmic Lab

The Canadian company Thalmic Lab has developed a gesture recognition armband called Myo Armband that can be seen in Figure 2.4. Due to its technical characteristics and easiness of use, this device has numerous applications and many articles in the literature evaluate its operating [64]. Some examples of applications can be gaming with virtual reality, a robot control interface and prosthetic control. In particular, BionIT Labs Company, in collaboration with the department of Innovation Engineering of the University of Salento has developed a prototype prosthesis, Adam's Hand, which Myo Armband directly controls.

Figure 2.4: Myo Armband [64].

This band consists of 8 EMG electrodes with a bipolar configuration that have the task of acquiring muscle activity, a 9-axis Inertial Measurement Unit (IMU, composed of an accelerometer, a gyroscope and a magnetometer) that evaluates the position of the forearm in space and a low-energy Bluetooth transmission module that has the task of transferring the acquired data to the electronic devices with which it is connected. The sampling frequency of this device is 200 Hz. Also, inside the band, there is a vibration motor that provides feedback to the user depending on the intensity and duration of the vibration (e.g. a low battery warning or a failure). The microcontroller inside Myo Armband is Freescale Kinetis ARM

Cortex M4 and the Bluetooth data transmission chip is BLE NRF51882. In one of the 8 compartments of the armband, there is a micro-USB connector that has a dual function, first, it serves to recharge the battery (there are 2 lithium batteries 3.7 V -260 mAh) and secondly, it permits to charge the firmware on the MCU.

2.3.3 3DC Armband

3DC Armband, designed by Laval University's Biomedical Microsystems Laboratory and shown in Figure 2.5, is a wireless bracelet used to make hand gesture recognition [65]. In their work, they built a new dataset by capturing data from 22 healthy patients who were asked to perform 11 hand/wrist movements, the subject in the analysis was standing with the forearm parallel to the floor, and evaluating the developed system, they compared their results with the Myo Armband, explained earlier. The armbands were applied simultaneously to the patient's forearm with the Myo more proximal to the elbow than the 3DC. Several classifiers with different input signals were used to evaluate performance; in particular, 3 data types were used, Baseline feature sets, raw EMG signal and features extracted in time and frequency domain. For the first type, the classifier used is the linear discriminant analysis (LDA) classifier, while for the other 2, a ConvNet classifier was used. The results showed how the best performance for both armbands is that the ConvNet classifier had the raw EMG signal as input. It was achieved an average accuracy of 89.47% for 3DC and 86.41% for Myo Armband. In the case of the LDA classifier, the average accuracy was 84.82% and 80% respectively.

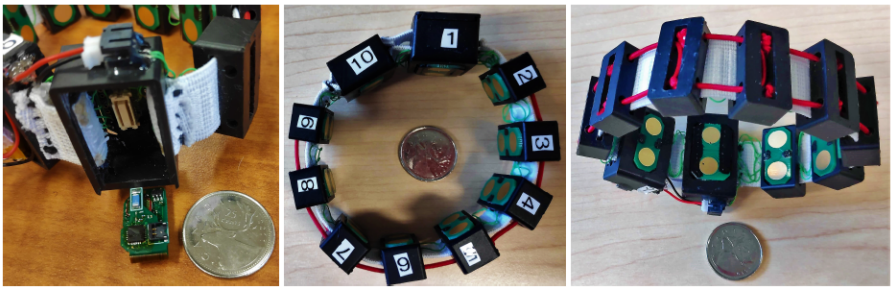

Figure 2.5: 3DC Armband [65].

3DC Armband is a 3D printed wireless capture system. As a result, this leads it to have a low price (~150 USD). The band is characterized by 10 bipolar acquisition channels consisting of dry electrodes, a 9-axis inertial unit of measurement (accelerometer, gyroscope and magnetometer) and a data transmission unit. The sampling frequency is 1000 Hz and the signal is filtered by a band-pass filter in the range of 20-500 Hz. Looking at its structure, the band consists of 2 main components, the first includes the PCB that has the task of acquiring and processing the EMG signal, the second includes the 3D container that acts as a box for electronic

components. Finally, there is a low-power, low-power microcontroller unit from Texas Instrument, a 100-mAh LiPo battery and a low-power transceiver. The total weight of the armband is 63 g.

2.3.4 Wearable biosensing system for sEMG

[66] has proposed a wearable device to perform gesture recognition that uses a surface electrode array to acquire the sEMG signal and that allows training and updating of the recognition algorithm during its use. Unlike the Armband described above, this device is characterized by a different electronic, it is a hybrid system consisting of flexible electronic for acquisition sensors and a rigid sensor for signal processing, it's possible to see this in Figure 2.6. The flexible part allows a mechanical flexion of the electronics that permit to have a better adaptation to the physiognomy of the forearm. At the same time, in the rigid sensor, it is loaded the classification algorithm. In detail, the system consists of a high-density electrode array. There are 64 electrodes in Ag/AgCl representing the 64 single-ended acquisition channels, to improve adhesion it is applied a conductive gel to each electrode. The HD electrode array is connected to a miniaturized printed circuit board (PCB). The system uses a low-power custom application-specific integrated circuit (ASIC) to collect the sEMG data for classification. The sampling frequency of the system is 1 kHz, the device is connected to a computer via Wireless and it is powered by a 3.7 V 240 mAh lithium-ion battery. The device's overall size is 29.3 cm x 8.2 cm and the total weight is 26 g. The system used to classify is Hyperdimensional (HD) Computing which relies on a data type called hypervectors. For initial validation of the system, that was acquired data from five patients and the classification went offline. An interesting aspect of this work is the sensor's ability to update the learning algorithm during an online application to considering the variations that may be during the acquisition of the sEMG signal like sweating, fatigue and electrode displacement. High accuracy was obtained when was done 21 gestures classification from two subjects, this is equal to 92.87%, with a recovery of 9.5% due to the update of the model in response to changes during the acquisition.

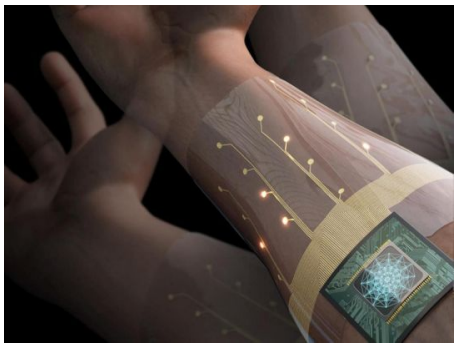

Figure 2.6: HD wearable biosensing system.

Chapter 3

Acquisition System

With the aim of developing a low-power wearable device to classify hand gestures, as defined in the first chapter, to use the EMG signal since it contains a lot of information and therefore has a high computational cost. Still, want to use the ATC signal, defined in section 1.3. In this thesis work, however, the ATC signal was not sent to a device after an hardware extraction, but has been calculated via software following an EMG signal acquisition via an A/D converter, being the hardware system still to be completely designed. In particular, a board was used to acquire the EMG signal that was given as input into an A/D converter, in which output was analyzed via software using MATLAB®. The ATC was extracted, and also other parameters are extracted, such as features extraction, PSD of the signal, and the signal-to-noise ratio of muscle activations. The acquisition system [48] is explained in detail below.

3.1 Printed Circuit Board (PCB)

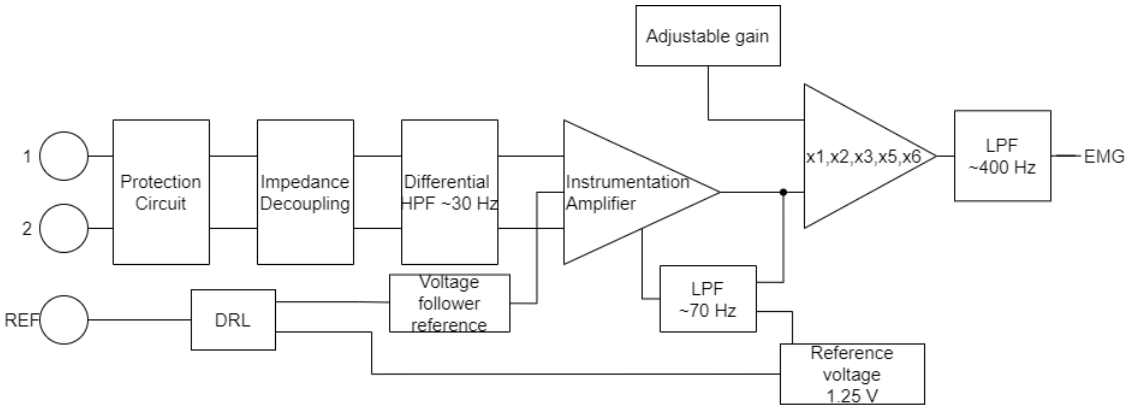

Figure 3.1: Schematic of sEMG acquisition chain.

The EMG signal has been acquired with bipolar mode, as can be observed on the left side of Figure 3.1, *"1"* and *"2"* represent the sampling electrodes while *"REF"* means the reference electrode. In Figure 3.1, it is also possible to observe the block "DRL", which is optional; in particular, welding some pins on the PCB there is the possibility to insert or not insert the part of the circuit containing the DRL. If you decide to use the board without the DRL to the reference will not arrive the output of the DRL, but it arrives the reference voltage. To evaluate the board's performance, EMG signal acquisitions were made for both the PCBs, that with DRL and that without the DRL.
In the block diagram above, the final output is represented by the EMG signal; in reality, the boards used for signal acquisition had already incorporated the possibility of generating TC events. Consequently, the EMG signal represents one of the two inputs of the voltage comparator, the threshold gives the other input that the board calculates for each acquisition channel. At the output of the comparator, there is the TC event. The board transfers TC events to a microcontroller with the use of wires. The microcontroller has also integrated a Bluetooth transmission antenna that allows the ATC parameter transmission to a PC. Figure 3.2 shows the complete printed circuit board.

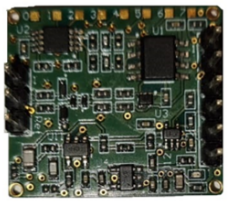

Figure 3.2: PCB: 22mm x 25mm.

3.1.1 Protection Circuit and Impedance Decoupling

The protection circuit has the task of protecting voltage-sensitive PCB components from transient voltage events and the accumulation of electrostatic dicharges, ESD, frequent in integrated circuits of electronic equipment. It consists of low dispersion switching diodes, protective diodes, and diode arrays. Also, there are ferrite microspheres that act as resistances to noise frequencies reducing the possibility of resonance and leaving the signal waveforms unchanged.
The decoupling of the impedance is applied to decouple the output from the input. It is composed of Voltage Follower and is located at the beginning of the system in order to have at the entrance of the circuit the same signals taken from the electrodes.

3.1.2 Differential High Pass Filter

The signals coming out from the voltage followers defined above are applied to a first high pass filtering. In particular, a differential high pass filter of the second order is applied. That is a passive filter because there are no active components, like op-amps. As shown in Figure 3.3, it is composed only by R and C. This filter is used to reduce the noise introduced by motion artifacts during signal acquisition.

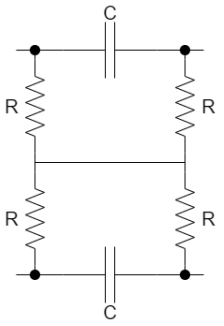

Figure 3.3: Differential HPF.

The cutting frequency is defined as:

$$f = \frac{1}{2\pi RC} \tag{3.1}$$

R=10 MΩ and a *C=470 pF* are selected, so the cutoff frequency is *f=33.86 Hz*.

3.1.3 Instrumentation Amplifier

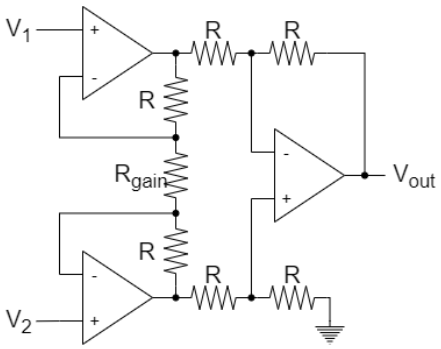

Figure 3.4: Instrumentation Amplifier

The instrumentation amplifier, shown in Figure 3.4, works like a differential amplifier but consists of an additional pair of amplifiers that improve the input impedance.

To define the output signal's gain, it's not necessary to change all the circuit's resistances. Still, once you have chosen the component that meets the project's specifications, it is enough to select the R_{gain} to define the total gain. In this case, the selected instrumentation amplifier is the *INA333* from Texas Instruments, whose gain is defined as:

$$G = 1 + \left[\frac{100k\Omega}{R_{gain}}\right] \tag{3.2}$$

In this case, R_{gain}*=200* Ω are selected so the Gain is *G=501*. The output of this amplifier is defined as:

$$V_{out} = G * [V_2 - V_1] \tag{3.3}$$

3.1.4 Second order multiple feedback low pass active filter

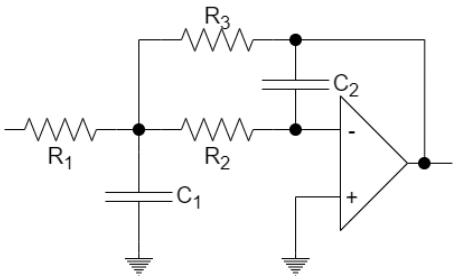

Figure 3.5: LPF

The output of the filter is used as the INA's reference. That represents the rejection of the common way; in particular, it allows rejecting certain low-frequency voltages introduced by the INA itself. The circuit diagram is shown in Figure 3.5. The cutoff frequency is defined as:

$$f = \frac{1}{2\pi\sqrt{R_2 R_3 C_1 C_2}} \tag{3.4}$$

In this case, R_1*=*R_2*=*R_3*=150 k*Ω, C_1*=33 nF* and C_2*=6.8 nF* are selected, so the cutoff frequency is equal to *f=70.83 Hz*.

3.1.5 Adjustable Gain

With this PCB, there is the possibility to increase the board's gain simply by varying the gain selector. That allows setting an adjustable gain on the board. In particular, it is possible to increase the gain by selecting one of the following multiplications: *x1 (500 V/V), x2 (1000 V/V), x3 (1500 V/V), x5 (2500 V/V), x6 (3000 V/V)*. By default, the adjustable gain is set to *x1*.

3.1.6 Second order Sallen-key low pass active filter

As Active LPF, this PCB uses the Sallen-key low pass filter, which is an active filter of the second order very widespread due to its simplicity.

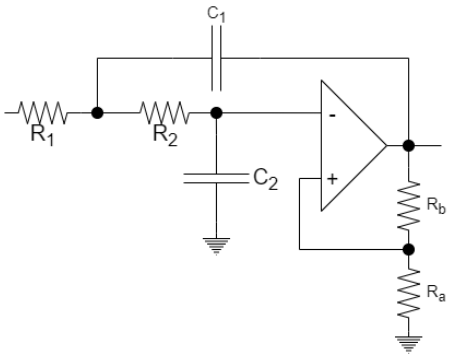

Figure 3.6: LPF

Looking at Figure 3.6, the gain is defined as:

$$k = 1 + \frac{R_b}{R_a} \tag{3.5}$$

In detail, at this level in this printed circuit board you want a unit gain, therefore, a component characterized by R_b=*0* Ω, R_a=*DNP*, has been selected. In this case, R_1=R_2=*27 kΩ*, C_1=*22 nF* and C_2=10 nF are selected. The cutoff frequency is defined as:

$$f = \frac{1}{2\pi\sqrt{R_1 R_2 C_1 C_2}} \tag{3.6}$$

With the component selected the cutoff frequency is equal to *f=397.42 Hz*.

3.1.7 Driven Right Leg (DRL) circuit

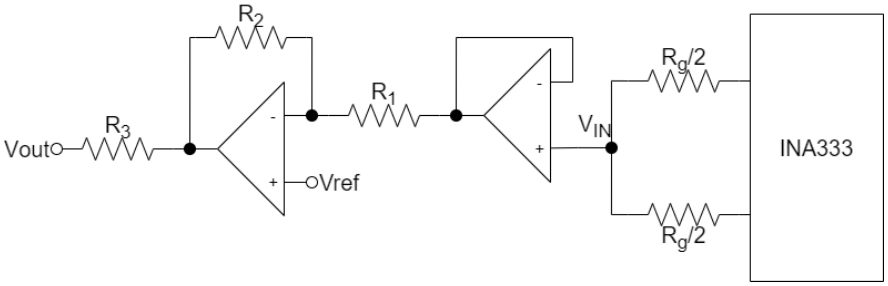

Figure 3.7: DRL

The Right Leg Circuit (DRL) is a circuit known for the acquisition of biological signals such as EMG, EEG, and ECG. Normally this circuit is added to the signal amplification chain to reduce interference in a common way; as shown in Figure 3.7, where the V_{IN} is taken from the instrumentation amplifier. In particular, DRL is used to reduce common-way noise on the skin and match the body's reference potential to the circuit reference voltage. In this case, R_1=R_2=*12 kΩ*, R_3=*330 Ω* and R_g=*200 Ω* are selected. The output voltage of the DRL circuit go to reference electrode and it is calculated as:

$$V_{out} = -V_{IN}\frac{R_1}{R_2} + V_{ref}(1 + \frac{R_1}{R_2}) \tag{3.7}$$

3.1.8 Voltage Comparator

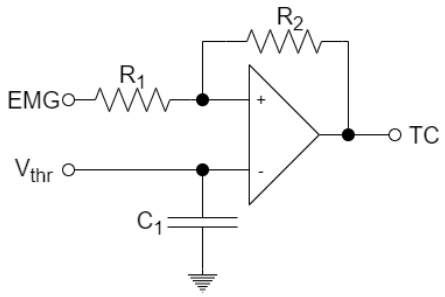

Figure 3.8: Voltage Comparator

The voltage comparator, shown in Figure 3.8, is used to generate a TC event. In particular, when the sEMG signal is greater than a certain threshold, the comparator output signal will be at a high logical level, while in case it is lower, it will be at a low logical level.

$$\begin{cases} V^+ > V^- \rightarrow V_{TC} = H \\ V^+ < V^- \rightarrow V_{TC} = L \end{cases} \tag{3.8}$$

In this application, R_1=*10 kΩ*, R_2=*1 MΩ* and C_1=*100 nF* are selected.
The final output of this board is the TC signal. This signal is transmitted to a microcontroller (in previous studies it was used Apollo3 Blue by Ambiq Micro). Thanks to a Bluetooth antenna, it sends the ATC parameter to the computer.

3.2 Data Acquisition

The sEMG signal acquisitions were made using the NI DAQ USB-6259, a data acquisition system produced by National Instruments®. Multifunction I/O device consisting of 32 Analog Input 16-bit and 1.25 MS/s, 4 Analog Output 2.86 MS/s, 48 Digital Input/Output, two 32-bit counters/timers, and digital and analog triggering.

Figure 3.9: NI DAQ USB-6259

The NI DAQ, shown in Figure 3.9, is connected to a PC via USB, and an app developed by MATLAB®, defined as "Data Acquisition Live", was used to collect the data. This app, shown in Figure 3.10, after the setting of various parameters, allows to acquire the input signal of the board and save it in ".mat" format. After selecting the device used, it is necessary to set several parameters:

- *Channel*: Define the channel you want to capture; it has been selected AI0.
- *Measurement type*: automatically set to 'Voltage'.
- *Range*: Defines the measurement range, this can be setted from "± 0.10V" to "± 10V"; for the measurements made, it has been set between '± 5V'.
- *Coupling*: set automatically on 'DC'.
- *Terminal Configuration*: set to 'Single Ended', you can make acquisitions even in 'Single Ended non referenced' and 'Differential' mode.
- *Rate (scan/s)*: represents the sampling frequency, this can be setted from "0.1 Hz" to "1.25 MHz"; for all acquisitions, considering the range of sEMG signal, the sampling frequency has been set to 1000 Hz.

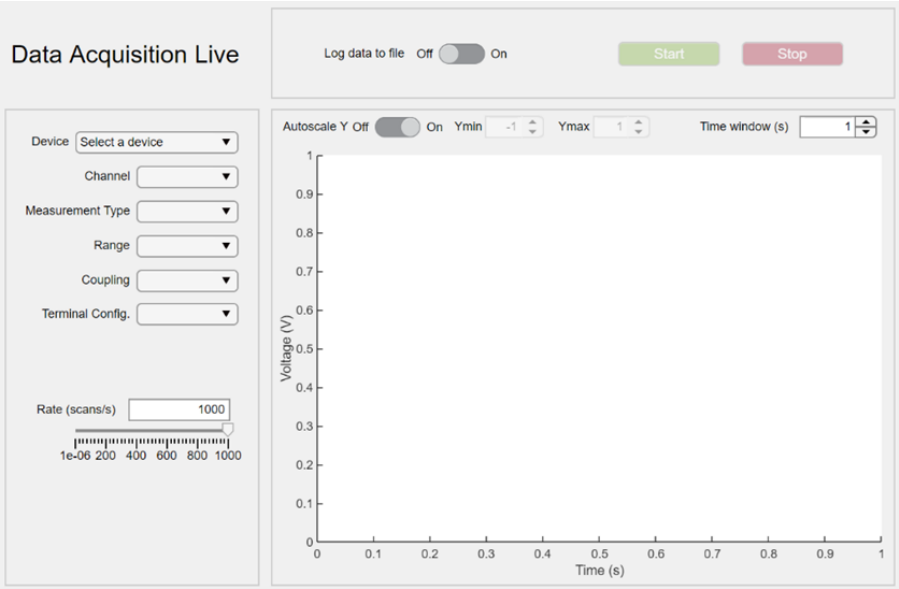

Figure 3.10: "Data Acquisition Live" by MATLAB®.

The NI DAQ, set as it has just been defined, has been used to acquire all sEMG signals, both in the preliminary evaluation related to the different types of dry electrodes and to evaluate the presence of DRL circuit onboard. With this app, only one Analog Input can be selected so you can capture a single channel. To make a simultaneous capture of multiple channels is necessary to use another application.

To standardize conditions during signal captures, a 3D model of a support was developed to allow inter-electrodic distance to be standardized. The support developed was printed with Formlabs Form 3D printer using "Black Resin".

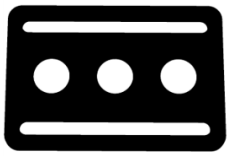

Figure 3.11: 3D printed support.

Looking at Figure 3.11, the outer circular holes represent the sampling electrodes, while the central one represents the reference electrode. Considering the circumferences' centers, the distance between the external holes and the central one is equal to 17.6 mm. Consequently, the distance between the centers of the two sampling electrodes is 35.2 mm. As defined in [67], an acceptable range distance between active electrodes is 18-36 mm. So, considering the printed support, the distance between the sampling electrodes is in the acceptable range for doing sEMG acquisition.

3.3 Signal-to-Noise Ratio (SNR)

The presence of noise always characterizes a biological signal; as a result, the acquired signal is defined as:

$$x(t) = s(t) + n(t) \tag{3.9}$$

Where *x(t)* represents the signal acquired, *s(t)* the biological signal, and *n(t)* the noise. The Signal-to-Noise Ratio (SNR) is calculated to assess the signal quality and it represents a reliability index of the recording. Low SNR values are a symptom of poor signal quality, and this makes subsequent processing difficult such as the detection of muscle activation, estimation of a feature extractions parameter. SNR is defined as the ratio of signal power and noise power:

$$SNR = \frac{P_s}{P_n} \tag{3.10}$$

Thus defined, the SNR value is between [0, $+\infty$). Moreover, it is possible to give a second definition by expressing the signal-noise ratio in terms of decibels (dB):

$$SNR_{dB} = 10 \cdot log_{10} \frac{P_s}{P_n} = 10 \cdot log_{10} \frac{\sigma_s^2}{\sigma_n^2} \tag{3.11}$$

In this case, the SNR_{dB} value is between $\pm\infty$. There are several other formulas for calculating the noise signal ratio that changes based on the type of signal (stationary or non-stationary) and the type of noise.

The SNR_{dB} of muscle activations was calculated for all acquisitions. As defined in Section 2.1, [44] define a limit greater than 5-6 dB in order to have robustness of ATC parameter. In order to increment the signal quality, in this thesis an acceptance value of 10 dB has been fixed to consider the signal suitable for an event-based extraction technique. An example of muscles activation selected for SNR calculation is shown in the figure below.

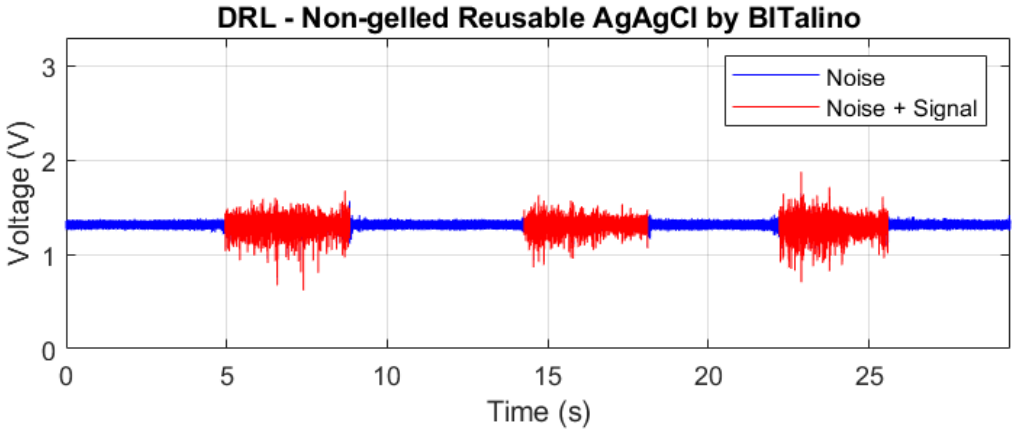

Figure 3.12: SNR of 3 different hand grasp movements

To calculate the SNR_{dB} as defined above, the noise power was calculated by considering the first 3 seconds of recording in which there was no muscle contraction (blue signal on Figure 3.12). To define the signal power, it is necessary to take another step. Considering the red signal of Figure 3.12, where there is both signal and noise, to calculate the square of the standard deviation only of the signal, it's necessary to calculate first the red one, and then the noise power calculate above is subtracted. In detail:

$$P_{Signal} = \sigma^2_{Noise+Signal} - \sigma^2_{Noise} \tag{3.12}$$

Now, with the signal power and the noise power, it's possible to apply the definition of SNR_{dB}. Considering the hand grasp movement performed, shown in Figure 3.12, the SNR_{dB} values calculated for the contractions are:

Contraction	**SNR_{dB}**
1st Activation	9.89 dB
2nd Activation	7.84 dB
3rd Activation	10.99 dB

3.3.1 Different Dry Electrodes

With the aim to develop an electromyographic armband the replacement of wet electrodes with dry ones is necessary. So, the first analysis involves three different types of dry electrodes, shown in Figure 3.13:

- **BiosignalPlux Conductive Lycra by MindtecStore**: conductive electrodes that can interact with ECG, EMG & EDA sensors. They are characterized by a diameter of 7 mm and that are coated with Lycra, this material is highly conductive. The price is about €85.00 for a package of 5 electrodes.
- **Non-gelled Reusable Ag/AgCl with velcro by BITalino**: compact electrode fitted with a convenient velcro strap that can interact with ECG, EEG, EMG & EDA sensors. Electrodes can be used multiple times with or without gel, they are characterized by a diameter of 5mm and the core is composed of Ag/AgCl coated polymer. The price is about €11.50 for a package of 2 electrodes.
- **Non-gelled Reusable Ag/AgCl by BITalino**: compact electrodes that can interact with ECG, EEG, EMG & EDA sensors. They can be used with or without gel and can be used multiple times. The core is composed of

Ag/AgCl coated polymer and there is an optional plastic rim to increase fixation area.The diameter of the core is equal to 7 mm and the acquisition are doing without the use of plastic rim. The price is about €12.50 for a package of 10 electrodes.

(a) MindtecStore (b) BITalino with Velcro (c) BITalino

Figure 3.13: Different dry electrodes.

The acquisitions involve 6 different movements: *brachial bicep contraction with a weight of 2 kg, hand grasp, wrist extension, wrist flexion, wrist radial deviation,* and *wrist ulnar deviation.*
For each of these movements, six contractions were done. To acquire sEMG signal, these acquisitions are made both for PCB with DRL and for PCB without DRL; the DRL circuit application evaluation is explained in section 4.1. In total, there are 72 contractions for each electrode evaluated. Figure 3.14 shows the results obtained.

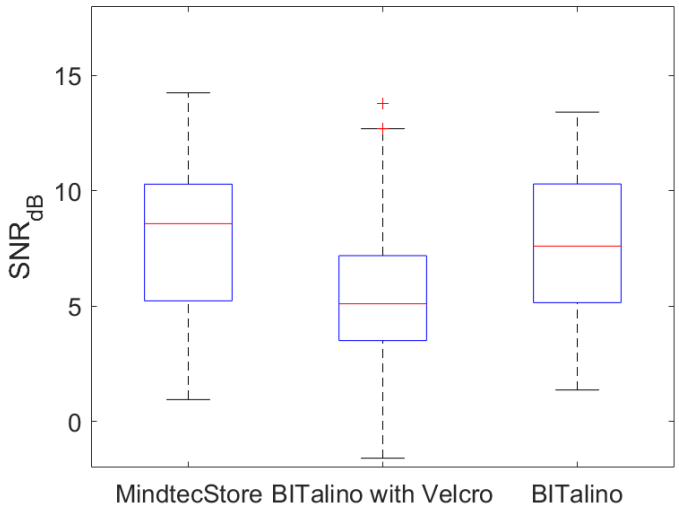

Figure 3.14: SNR_{dB} of three different dry electrodes

In the boxplot, there are all the SNR_{dB} calculated separated for the type of electrode. Looking the Figure 3.14 MindtecStore and BITalino suggest having better

results than BITalino with Velcro. To evaluate what is the one with the best results, a separation for the movement was done. In particular, applying the average of the six contractions in terms of SNR_{dB}, the different values obtained are shown in Table 3.1.

Table 3.1: SNR_{dB} of different dry electrodes. The values are expressed in dB.

Movement	**MindtecStore**	**BITalinoVelcro**	**BITalino**
Brachial bicep	9.27	8.49	9.48
Hand Grasp	5.43	4.05	7.40
Wrist Extension	11.15	7.27	8.20
Wrist Flexion	3.79	2.62	4.13
Wrist Radial Deviation	8.68	5.62	9.70
Wrist Ulnar Deviation	8.70	4.84	7.11

Looking at Table 3.1, Non-gelled Reusable Ag/AgCl by BITalino has the major number of highest SNR_{dB} values considering the different movements, in particular for *brachial bicep, hand grasp, wrist flexion* and *wrist radial deviation*. Considering the last two movements, *wrist extension* and *wrist ulnar deviation*, BiosignalPlux Conductive Lycra by MindtecStore has the highest values.
BiosignalPlux Conductive Lycra by MindtecStore has good performance, but it is very expensive respect the other one. So, Ag/AgCl BITalino was selected and used for all the acquisition doing in the rest of the thesis work.

Chapter 4

PCB Evaluation

Once defined dry electrodes to use, the PCB was tested. At this point, the objective is to increse the SNR_{dB} in order to have higher quality of sEMG signal; this is necessary to apply the ATC technique.
Different movements were performed and more sEMG signals were acquired with the configuration of data acquisition defined in Chapter 3.

4.1 PCB without DRL vs PCB with DRL

With the aim to increase the sEMG signal quality, the application of the Driven Right Leg (DRL) circuit available onboard was tested. With wet electrodes, this could not be necessary because the sEMG signal is characterized by high quality. Considering the disadvantages of dry electrodes, such as difficult fixing on the skin, the DRL circuit application can reduce the noise introduced by the dry ones. DRL circuit is used as a connection between the signal source and the amplifier, as shown in Figure 3.7. In particular, it reduces the noise on the skin by driving the common-mode voltage from the instrumentation amplifier to the reference electrode's potential; it matches the body's reference potential to the circuit's reference voltage. Welding some pins, the DRL circuit available onboard was integrated into the PCB.
For the two different configurations of the PCBs, some movements were performed. In particular *hand grasp, open hand* and *wrist extension.*
For each movement, the isometric contractions were performed seven times. In total twenty-one contractions were doing for each PCB's configuration. The results obtained doing a separation only with respect to the DRL circuit are showns in Figure 4.1.

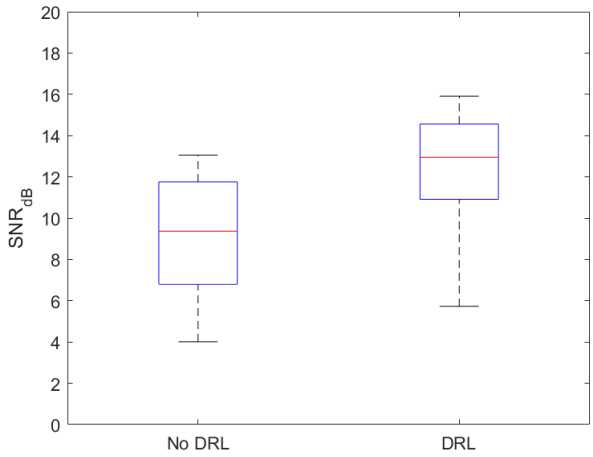

Figure 4.1: No DRL vs DRL evaluation

Looking at the boxplot the presence of the DRL circuit leads to having a higher SNR_{dB} values both in terms of distribution and median values.

In addition, to evaluate the performance a further distinction is made with respect to the movements performed. Producing multiple contractions permits to have more data to analyze and has the advantage of extracting the SNR_{dB} mediated on the seven ones. The results obtained are reported in Table 4.1.

Table 4.1: SNR_{dB} of different movement, comparing PCB with DRL and without DRL. The values are expressed in dB.

Movement	**No DRL**	**DRL**
Hand Grasp	6.03	9.49
Open Hand	11.24	13.88
Wrist Extension	10.24	13.83

For all the movements, the highest values are obtained with the PCB containing the DRL circuit. Furthermore, the averaged values are higher than 10 dB for *open hand* and *wrist extension*. That is an important result because 10 dB is the minimum value acceptable in considering the sEMG signal as a good quality signal. In this case, there is a small increment of SNR_{dB} with the DRL circuit.

However, the effect of the DRL circuit can also be observed in the frequency domain. Calculating the Power Spectral Density (PSD) of the signals, there is a possibility of seeing a decrease of noise, which is shown in Figure 4.2. Looking at the PSD, there is an important decrement of noise artifact thanks to the presence

of DRL. Each PCBs are built to eliminate the network interference at 50 Hz, but the network interference harmonics are present. That is a problem considering the EMG band (0-500 Hz).

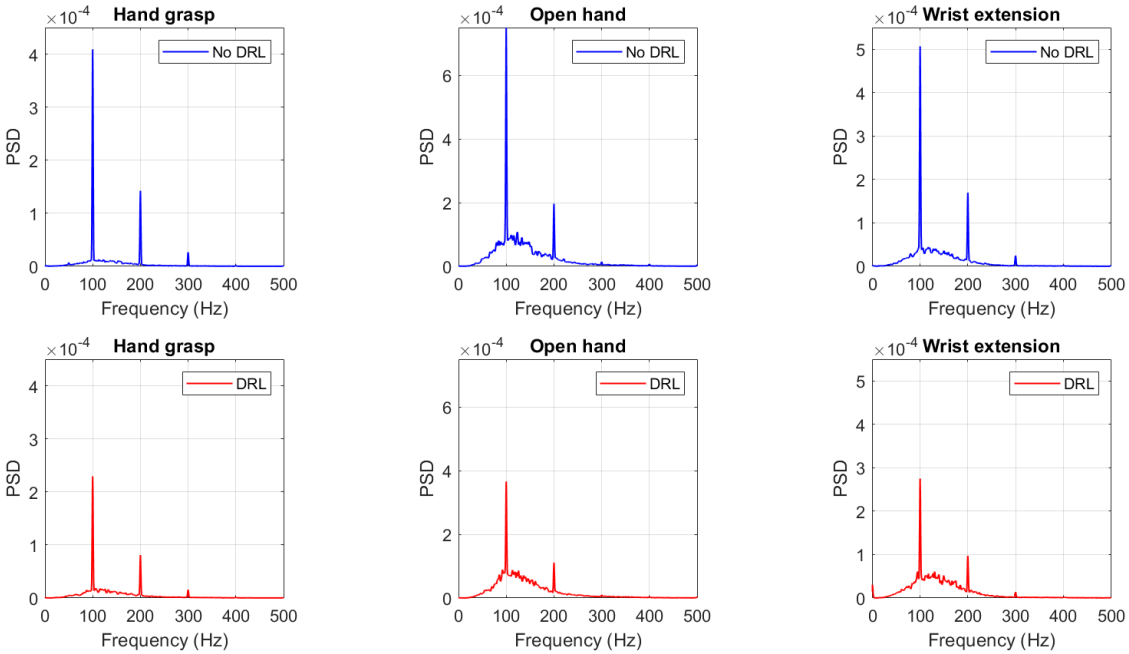

Figure 4.2: Power Spectral Density

Reducing the common-noise with DRL application, the effect of harmonics of the network interference is lower. So, Driven Right Leg's presence on the board is a good solution both in terms of SNR_{dB} both in terms of signal information in the frequency domain. For the analysis in section 4.2, PCB with DRL was selected to be used.

4.2 Gesture Recognition

In this section was make sEMG signals acquisition of various forearm movements. The idea is to reproduce the movements and acquire signals in the same way that can be done acquiring signals using an armband for gesture recognition. At the moment, with the PCB, there is the possibility to acquire only one signal for time. The acquisition channel is positioned in correspondence with the first muscle. A sequence of movements was done; in particular for each movement an activation of 5 seconds was performed and between each activation, there were 5 resting seconds. Finally, the position of the acquisition channel was changed in correspondence to another muscle.
With the aim to have an armband composed of seven acquisition channels and to

recognize seven active gestures, seven acquisition of sEMG signals were made in the different positions. The acquisition channel is positioned at 1/3 of the arm starting from the elbow, as suggested in [49]. With these configurations, the measurements can represent the type of sEMG signal for gesture recognition, but there are some problems. The acquisition channels must be placed simultaneously on the arm. Acquiring only one channel per time, the starting and the ending point of the gestures task doesn't correspond considering the various acquisition channels and it is necessary to manually align the activation.

4.2.1 Movement performed

Seven active gestures made by the left forearm were performed besides the idle state. In detail:

- **Idle state**: the muscles are relaxed, the hand is still, and the forearm rests on a table without gravity to be contrasted.
- **Wrist extension**: the most used muscles for doing this gesture are the *extensor carpi radialis longus*, the *extensor carpi radialis brevis* and *ulnaris* together with some deep muscles. This movement consists to move the back of the hand towards the distal forearm.
- **Wrist flexion**: the most used muscles for doing this gesture are *flexor carpi radialis, palmaris longus and flexor carpi ulnaris*, as well as *flexor digitorum superficialis* and *profundus*. This movement consists to move the hand palm towards the inner arm.
- **Wrist radial deviation**: the most used muscles for doing this gesture are *abductor pollicis longus, flexor carpi radialis, extensor carpi radialis longus* and *brevis*. This movement consists to move up the hand follow the thumb direction.
- **Wrist ulnar deviation**: the most used muscles for doing this gesture are *extensor carpi ulnaris* and *flexor carpi ulnaris*. This movement consists to move down the hand to the little finger direction.
- **Hand grasp**: the most used muscles for doing this gesture are *flexor digitorum* and *palmaris longus*, together with many intrinsic muscles of the hand. This movement consists to close all the fingers in the direction of the hand palm.
- **Pinch grip**: the most used muscles for doing this gesture are *flexor digitorum superficialis, flexor digitorum profundus, palmaris longus*, and *flexor pollicis brevis*, together combinated with the adducting for of the *adductor pollicis*. This movement consists to doing a grip between the palmar surface of index finger and the thumb. This movement consists of doing a grip creating pressure between the palmar surface of the index finger and the thumb.

- **Open hand**: all the forearm muscles are involved for doing this movement, in particular the *extensor digitorum*. This movement consists to fully extend the hand maintaining the open palm.

The sequence of movements performed is composed in the order of the gestures described above and it is shown in Figure 4.3. 5 resting seconds separate 5 seconds of muscle contraction.

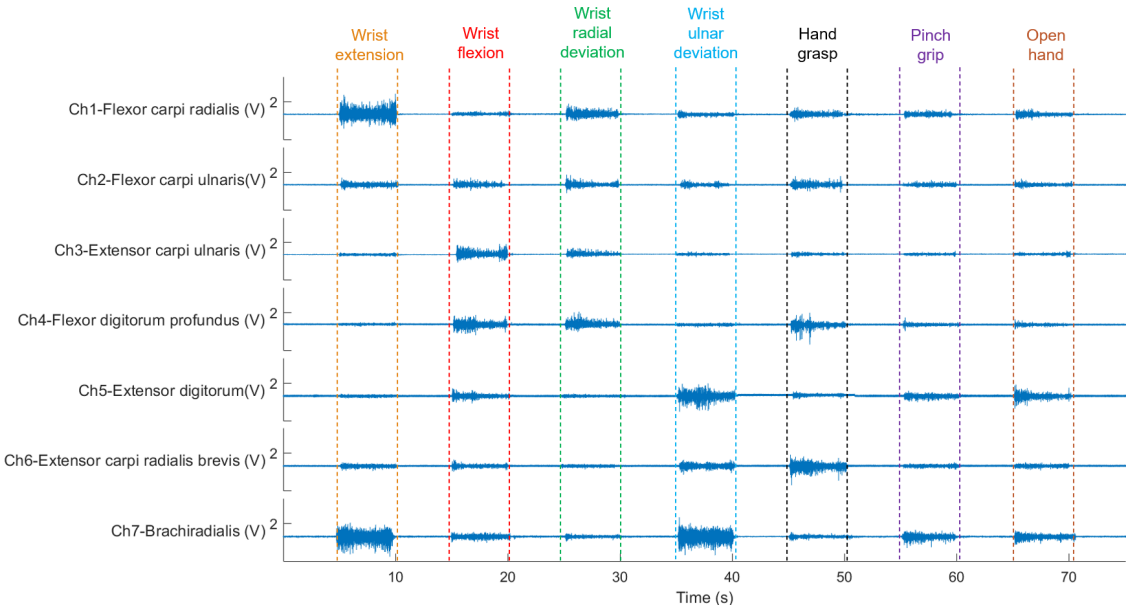

Figure 4.3: Towards an armband: sequence of sEMG signals for gesture recognition.

Considering all movements, for each acquisition channel the SNR_{dB} was calculated in order to give information on muscle activation. The results are reported in Table 4.2. Small and negative values are due to a small activation; in contrast, the highest values represent the muscle mainly active for the execution of the specific gesture.

Table 4.2: SNR_{dB} of forearm muscles. The values are expressed in dB.

Channel	**Extension**	**Flexion**	**Radial**	**Ulnar**	**Grasp**	**Grip**	**Open**
Ch1	22.97	8.42	18.19	10.57	15.77	13.40	13.52
Ch2	11.51	11.26	11.70	9.59	13.59	8.85	8.97
Ch3	10.37	21.18	16.70	10.89	12.21	10.67	11.02
Ch4	-1.01	12.30	11.91	1.52	12.06	3.36	2.98
Ch5	-2.69	5.16	-5.62	12.21	0.14	5.20	7.18
Ch6	6.12	5.05	1.81	9.83	13.82	3.92	5.10
Ch7	20.15	10.46	4.45	20.15	5.62	12.93	11.93

4.2.2 ATC extraction

With the final device, the ATC signal will be extracted using the PCB voltage comparator to generate TC events and the MCU to transfer the averaging number of over-crossing inside a fixed time window. In this application, the ATC signal was extracted via software; different steps were done to do this. After the sEMG acquisition, the most important step is to define the threshold.
In particular, the first and the last 3.5 seconds of the signals are considered to calculate the threshold; this signal was called *"noise"*. In this part, there is only the idle state and there are no activations. Considering the "noise" signal the peaks were found, which are called "*peak*". That is necessary to calculate a first threshold defined as:

$$thr = mean(peak) + 3 \cdot std(peak) \tag{4.1}$$

Considering how the final device calculate the threshold, is necessary to add a term called "*hysteresis*", equal to 15mV. The final threshold is defined as.

$$threshold = thr + hysteresis \tag{4.2}$$

Once defined the threshold, the next step consists of extracting the TC events. Making a comparison between the sEMG values and the threshold, if the first one is higher than the second one, the TC event is set to 1, otherwise is set to 0. Finally, to extracting the ATC signal, the number of TC setting to 1 inside a fixed time window of 130 ms is counted. The results obtained considering the signals acquired in Section 4.2.1 were shown in Figure 4.4.

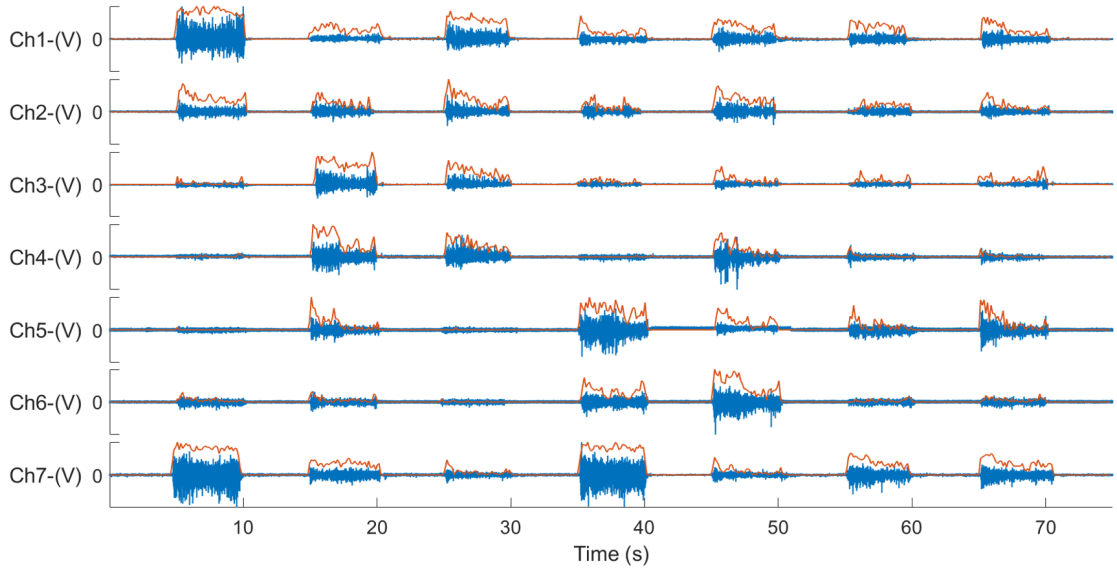

Figure 4.4: ATC extraction for gesture recognition.

Looking at the Figure 4.4, where the orange signals represent the ATC ones, it can be observed how the ATC trend follows the trend of the sEMG signal. To overlap the signals, each ATC signal has been normalized with respect to his maximum. The ATC signals represent the input for doing gesture recognition. If supervised learning is used, for the training of the algorithm is necessary to label the signal defining different labels in correspondence of the different gestures done.

4.3 Improved PCB

The research team has developed an improved acquisition board in which the MicroController Unit (MCU) is positioned directly on the board. That allows an ATC signal extraction and transmission from the board without going through an external microcontroller. That is an important aspect in order to develop a wearable device. Furthermore, the MCU permits to transfer data via Bluetooth, both ATC and sEMG signals. The transmission via Bluetooth leads to an incrementation of SNR_{dB} because the board's connections reduce the noise previously introduced through the DAQ system. In Figure 4.5, the improved PCB is shown.

Figure 4.5: Improved PCB: 20.5mm x 33.2mm.

The main differences of the improved PCB compared to the starting one are:

- **Microcontroller Unit**: as mentioned above, the microcontroller is located directly on the printed circuit board. Considering its presence, the possibility to connect to the board a button for the resetting of MCU is also added.

- **Snap electrode socket**: at the bottom of the board, there is a compartment where you can connect the electrode connectors directly to the board. That is especially important as it reduces the moving artifact during signal capture. In the previous case, the sockets were connected to the board via floating wires. Therefore, during the movement's execution, there was the possibility to have a movement of the wires that could cause distortions of the signal.

- **Size**: the size of the starting board was 22mm x 25mm; the improved one, since it must also contain an MCU, has a longer length and its size is 20.5mm x 33.2mm.

- **Micro USB**: allows you to connect the board directly to a PC. In addition, when the battery is connected to power the board, if you connect the board to a PC, it is possible to recharge the battery thanks to an internal charging circuit.

- **Switch button**: it turns the PCB on and off when activated.

Also with the improved PCB, there is the possibility to insert or not the DRL circuit onboard by welding some pins; the evaluation about that can be seen in Chapter 6.

4.3.1 EMG signal

In this section, the acquisitions were made only with the PCB without the DRL circuit and the sEMG signals were acquired using the NI DAQ set as defined in Chapter 3. The transmission of data via Bluetooth was used in Chapter 6. The sEMG signal detection was made with wet and dry electrodes. Considering the SNR_{dB} and the PSD in the frequency domain, even if with the wet ones we expect to find better results than the dry ones, acquiring with both systems allowed us to make a comparison with the results obtained.
A single forearm gesture was tested, in particular the right *wrist extension*. During each acquisition, seven muscle contractions of five seconds were done; between each contraction, there were five seconds of resting phase. Considering the Range Of Motion (ROM) of the gesture, the acquisitions were made in four various positions. The forearm is perpendicular to the arm, and regarding the different positions is considering the angle generated between the longitudinal axis of the forearm and the hand in the sagittal plane. In details:

- *Rest*: the muscles are relaxed, the hand is still, and the forearm rests on a table without gravity to be contrasted. The angle between the two segments is equal to 0°.

- *Minimal extension*: the muscles are contracted with minimal effort. The angle between the longitudinal axis and the hand is in the range 0°-30°.

- *Normal extension*: the muscles are contracted with a normal effort. The angle between the longitudinal axis and the hand is in the range 30°-60°.

- *Maximal extension*: the muscles are contracted with a maximal effort. The angle between the longitudinal axis and the hand is in the range 60°-90°.

The sEMG signals acquired are shown in Figure 4.6, where the blue signal represents the sEMG ones and the orange the ATC ones.

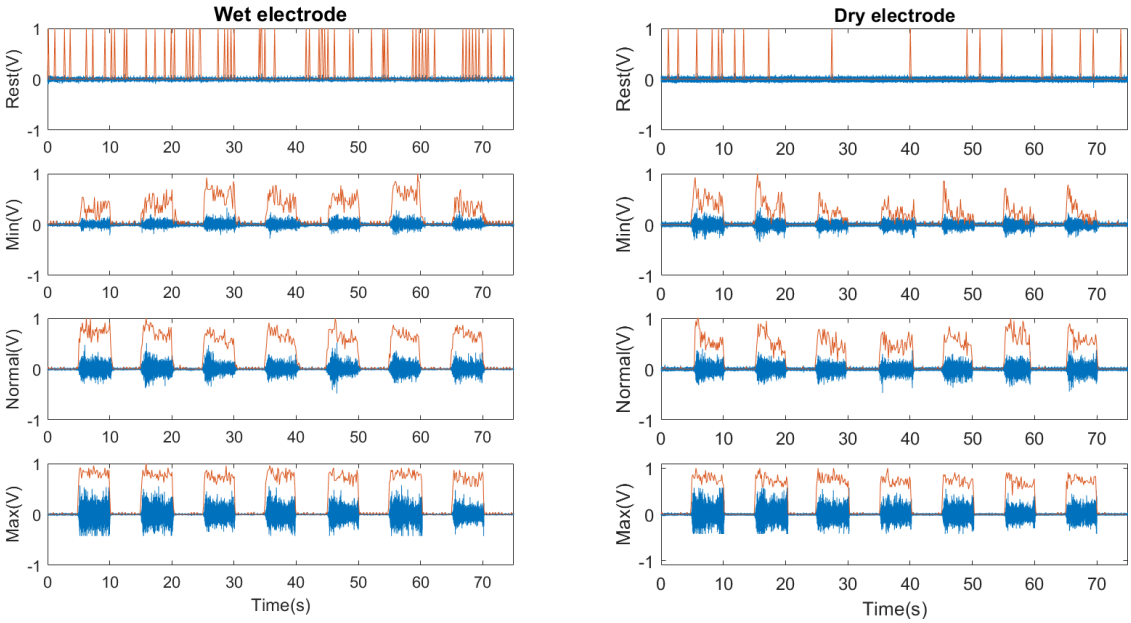

Figure 4.6: sEMG and ATC signals: Wet vs dry electrode.

Looking at Figure 4.6, both for wet and dry electrodes, the first signal is characterized by the presence of some peaks in the ATC signal due to the software calculation of the threshold. Sometimes there is a single sEMG value higher than the threshold that generates a single TC event observed when the ATC is extracted.

Considering the frequency domain, in Figure 4.7 the PSD of the sEMG is reported. Making a comparison between signals acquired with wet electrodes and dry ones is evident the disadvantages introduced by the dry electrodes. With the wet is not observed a critical component related to network interference and his harmonics, which can be seen well with dry ones where the network interference harmonics are evident.

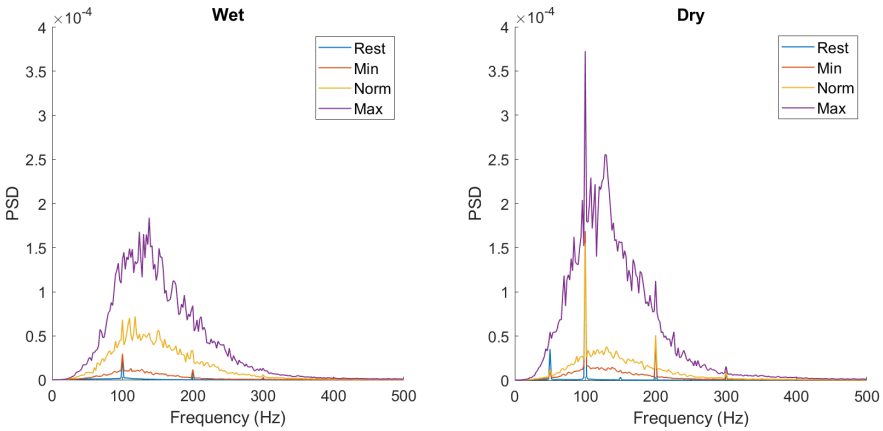

Figure 4.7: Power Spectral Density (PSD): Wet vs dry electrodes.

Regarding the muscle activation during the different positions, the SNR_{dB} was calculated for each contraction. In Table 4.3 there are the results obtained by doing the average of the seven contractions for each position.

Table 4.3: SNR_{dB} of different wrist extension intensity, comparing wet and dry electrodes. The values are expressed in dB.

Movement	**Wet electrode**	**Dry electrode**
Rest	-4.64	-9.13
Min	8.96	6.89
Normal	17.65	12.09
Max	21.21	19.15

For each position, as stated before, the SNR_{dB} calculated for wet electrodes is higher than the dry ones. Furthermore, as the intensity of the effort increases, the value increases. The *resting* values are negatives due to the calculation process of SNR. Considering the *normal* and the *maximum* intensity of *wrist extension*, even with dry electrodes, values greater than 10dB are obtained. Indeed, considering the maximal wrist extension, the values are greater than 20 dB. So, the improved PCB results seem to demonstrate good quality for sEMG signal acquisition.

Chapter 5

Armband Design

In order to develop an electromyographic armband for gesture recognition, another important step is to design the CAD model. Considering the armbands present on the market, described in Section 2.3, two different models were designed.
The forearm circumference is an important aspect to consider during the design phase. The tool to take the body circumferences is an inelastic meter. The meter surrounds the body in the right areas, without girding (tightening the tissues) and making the meter adhere to the skin. The circumference of the forearm is measured from standing, starting with the arms at the sides. The forearm forms an angle of 90° with the arm; the hand palm is facing up. The measurement can be done proximal or distal. In order to position the armband at 1/3 of the forearm length starting from the elbow, it was considered the proximal values and grouped in 3 sizes.

Table 5.1: Forearm circumference. The values are expressed in cm.

Size	**Forearm circumference**
Small	18-22
Medium	22-28
Large	28-36

Looking the Table 5.1, the range of forearm circumference is between 18-36 cm in normal person without problem as anorexia and obesity. So, for the armband design, it is necessary to include some elastic connection to generate a wearable device for most people. The starting point is developing an armband composed of seven acquisition channels with bipolar configuration, connecting each other with some elastic part. The idea is doing gesture recognition with these seven acquisition channels. In particular, the movements that will be recognized are the ones defined in Section 4.2.1. The models were developed with Autodesk Fusion 360®.

5.1 3DC model

The first model is inspired by the 3DC Armband developed by Laval University's Biomedical Microsystems Laboratory, described in Section 2.3.3. The inspired model is characterized by ten acquisition channels where two of these have different dimensions due to battery presence. In this thesis work, the seven acquisition channels that composed the armband have the same dimension because they have a PCB, three sockets for electrodes and a battery inside each of them.
In the preliminary phase, the measurements of the various components were taken with the aim to create the model with the right dimension to include inside that all the components. Two parts compose the single acquisition channel:

- *case*, that represents the place where are inserted the electronic components;
- *cover*, closing part of the case.

In detail, the case and cover are shown in the following figures.

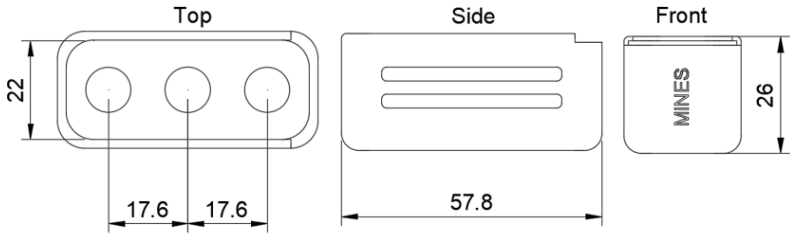

Figure 5.1: 3DC case: the measures are expressed in mm.

In Figure 5.1, the dimensions of the case are reported. In particular, length, height, widths and interelectrode distance are specified. The thickness of the wall is equal to 2 mm. Considering the side view, there is a hole in the middle of the case; the idea is to pass an elastic band in the hole to connect a box to another. Dry electrodes are inserted on the lower surface, where they make a clip connection with the sockets.

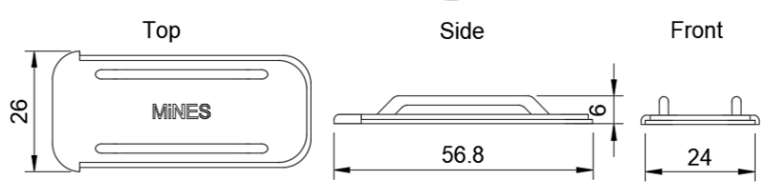

Figure 5.2: 3DC cover: the measures are expressed in mm.

In Figure 5.2 are reported the dimensions of the cover. In particular, length, height and widths are defined. The external part of the cover match with the rail of the box, closing its upper part. Cover closed with the case take the name of "box". Furthermore, in the upper part of the cover, a structure permits inserting another elastic band. The second elastic band has the functionality to press the box to the skin; so, press the electrode to the skin. This part is implement considering the limits of dry electrodes. In detail, considering the high electrode-skin impedance of dry ones, if the contact isn't well pressed, the acquisition signal is characterized by a lot of noise. The idea with the implementation of the second elastic band is to improve this aspect.
Inserting the electronic components inside the box, all together represent a single acquisition channel.

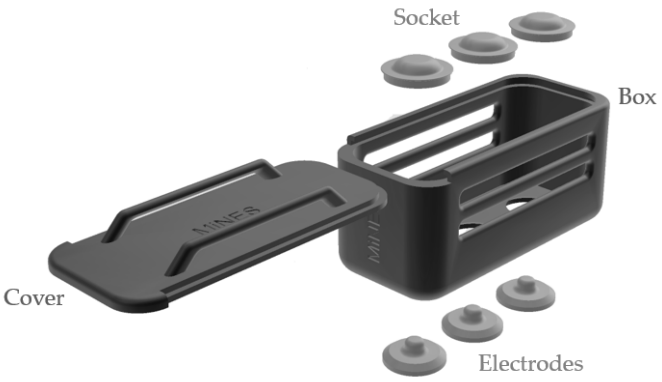

Figure 5.3: 3DC box.

Other than electrodes and sockets, the PCB and the battery are inserted into the case to compose a single 3DC box. The closing mechanism of the box is shown in Figure 5.3, it can be understand how the cover slides into the case rail. The idea is to print cover and box using the rigid "Black Resin" for the Formlabs Form 3D Printer.
For the design of 3DC model, an improvement of the box model was made. Seven acquisition channels characterize the final armband; so, for the designing is necessary to use, simultaneously, seven boxes. The box's position during the acquisition is standardized, as done in 4.2.1, to acquire the same muscle activation under a single channel when the subject does different movements.
For example, doing wrist extension that has a good component in terms of flexor carpi radialis activation, if you make acquisition between different subject for doing gesture recognition is not good to have the muscle under CH 1 in one case, while in the other one is under CH 4.
The standardized positions are:

- CH 1: *Flexor carpi radialis*

- CH 2: *Flexor carpi ulnaris*
- CH 3: *Extensor carpi ulnaris*
- CH 4: *Flexor digitorum profundus*
- CH 5: *Extensor digitorum*
- CH 6: *Extensor carpi radialis brevis*
- CH 7: *Brachioradialis*

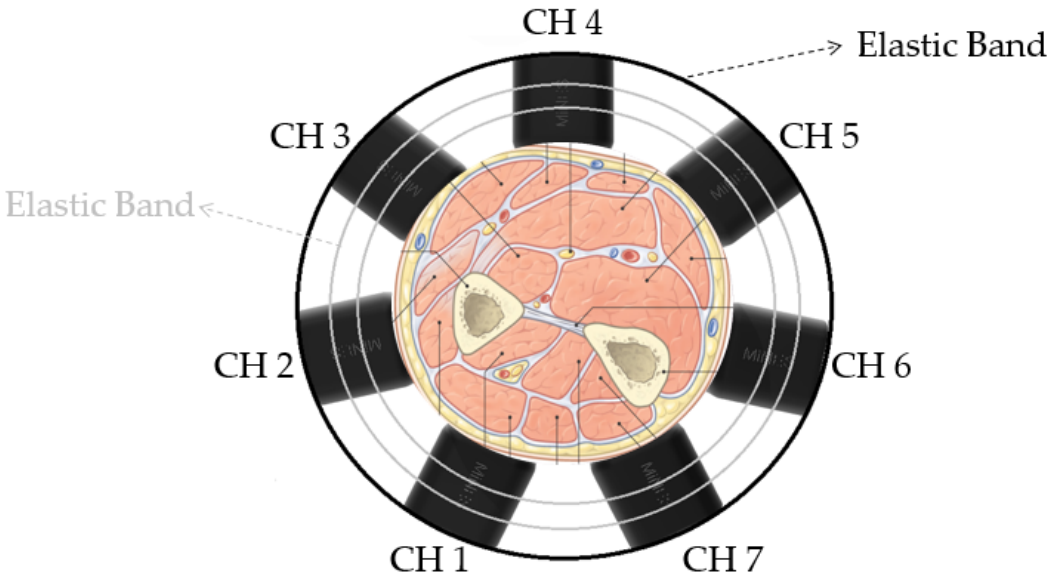

Figure 5.4: 3DC model.

Looking at Figure 5.4, the grey elastic bands represent the connection between the boxes (acquisition channels), while the black one represents the external band for press the electrode to the skin. Considering the width of a single 3DC case, equal to 26 mm, and imagining putting the seven ones next to each other, the total width is equal to 18.2 cm. Between cases, it is necessary to insert also the grey elastic bands. Assuming a small length equal to 1 cm, the global width of seven boxes + elastic band is equal to 25.2 cm. So, regarding the forearm circumference is hard to apply and standardize the 3DC model for all the people inside different size group. 3DC model was only designed; it wasn't printed with the Formlabs Form 3D printer.

5.2 MYO model

The second model is inspired by the Myo Armband of Thalmic Lab, described in Section 2.3.2. This one is more complex than the 3DC model defined above. Seven acquisition channels characterize the MYO model. The connection system isn't composed of some elastic bands, but a 3D support to connect the acquisition channels is designed. In this case, a single acquisition channel was printed with the Formlabs Form 3D Printer. After some prints, making the right adjustment, the acquisition system's final model has been designed, printed and tested, making sEMG signals acquisition. The results obtained are reported in Chapter 6.
In general, the MYO model can be divided into three parts:

- *Case*, as before, represents the place where all the components are inserted.
- *Cover*, closing part of the case.
- *Support*, system to connect all together the seven acquisition channels.

In detail, the schematic of the case, cover and support are shown in the following figures.

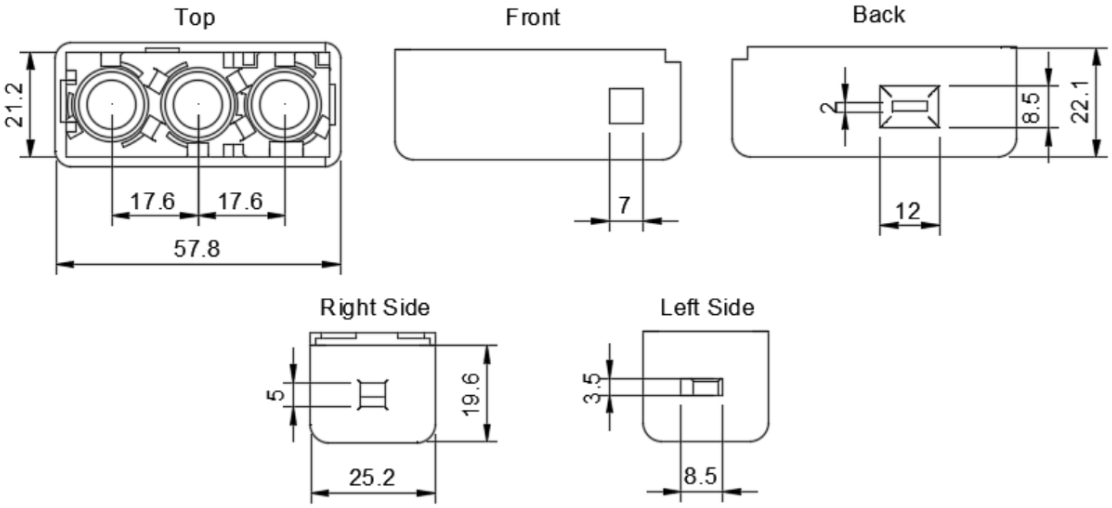

Figure 5.5: MYO case: the measures are expressed in mm.

In Figure 5.5, the dimensions of the case from a different point of view are reported. In particular, length, height, widths and interelectrode distance are specified. The thickness of the wall is equal to 2 mm. Considering the back view, the hole gives access to the switch button that turns "off" and "on" the improved PCB. In the left side view, the opening represents the possibility of connecting via micro USB the improved PCB. Furthermore, in the front view, the hole represents the place where

to insert the button for resetting the MCU. Finally, a gap on the right side view is inserted to let out some wires eventually.

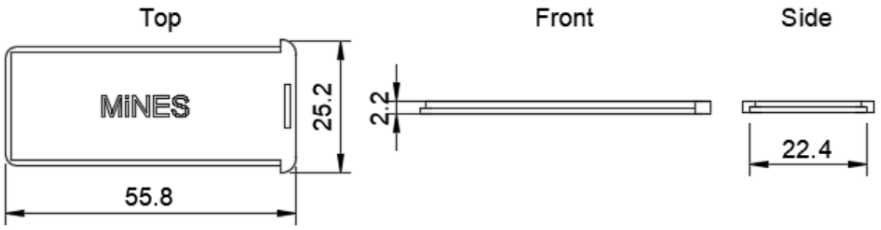

Figure 5.6: MYO cover: the measures are expressed in mm.

The MYO cover is very similar to the 3DC one. The differences are the dimensions and the absence, in the upper interface, of the gap for the elastic band's passing. In Figure 5.6, length, height and widths are defined. By threading the cover into the case rail, the system can be closed. As before, case together with cover takes the name of "box". The box part is printed using the "Black Resin" for the Formlabs Form 3D printer.

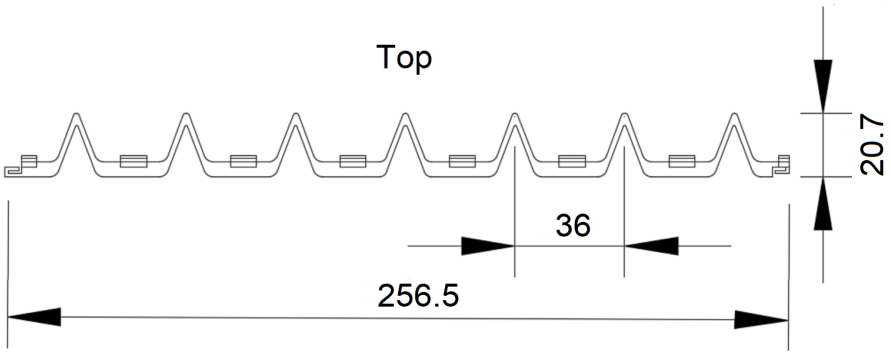

Figure 5.7: MYO support: the measures are expressed in mm.

In Figure 5.7, lengths and widths of MYO support are reported. The height is equal to 19 mm. Considering the height of the case, the support one is smaller in order to maintain the same contact surface between the case and skin; augmenting this section can be rent more difficult the wearability. Furthermore, moving the external part of the support is possible to close that in a circle representing the armband. With the support part was given the armband flexibility; so, the idea is to print MYO support using the "Flexible Resin" for the Formlabs Form 3D printer. The total length is equal to 25.65 cm. Regarding the forearm circumference, the model is in the acceptable range but is hard to apply the MYO model for all the people inside different size group. Some possibilities to solve this problem can be to reduce the PCB widths or reduce the distance between the boxes.

The single acquisition channel is defined as "MYO box". The MYO box's external part is composed of case and cover; the inside part is composed of all the components necessary to use for making sEMG acquisition with an embedded system. In detail:

- *Sockets and Electrodes*: in order to create the clip system, there are three sockets, one for each dry electrode.
- *Stoppers*: there are three stoppers different from each other for the place to be positioned. Looking the top view of Figure 5.5, stopper 1 is placed on the left opening, stopper 2 in the middle and stopper 3 in the right one. On the upper surface, there is an opening that allows each stopper to be positioned in the right position using a screwdriver.
- *PCB*: improved PCB defined before. It rests on supports inside the case and is fixed by hooks and battery holder.
- *Button*: pressing this button, the MCU present on the PCB was resetting.
- *Battery*: the rechargeable Li-Po battery used is the LP401230 produced by Cellevia Batteries. Characterized by a rated voltage of 3.7 V and capacity of 110mAh.
- *Battery holder*: support for the battery. It is inserted inside some holes of the MYO case and has also the task to fix the PCB inside the MYO Box.

Battery, button and sockets are connected to the improved PCB with the use of some wires. The different components, except battery, are shown in Figure 5.8.

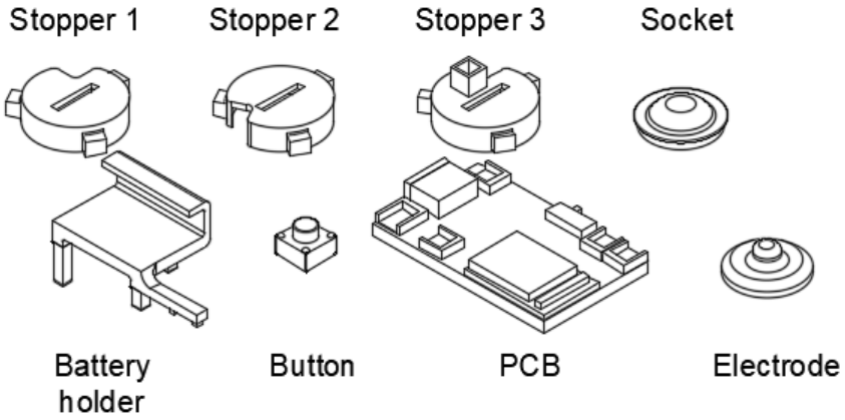

Figure 5.8: MYO component.

The lateral hole of stoppers allows the output of the wires soldered on the socket for the connection with the PCB. Stoppers were formed by three protrusions that

fit under some supports present in the case. Once they are in the correct position, the protrusions under the support generate a contrasting force that allows beating the electrode's push force on the socket. Furthermore, stopper 3 is composed of an empty pillar on the upper surface; this one matches with the battery holder pillar.

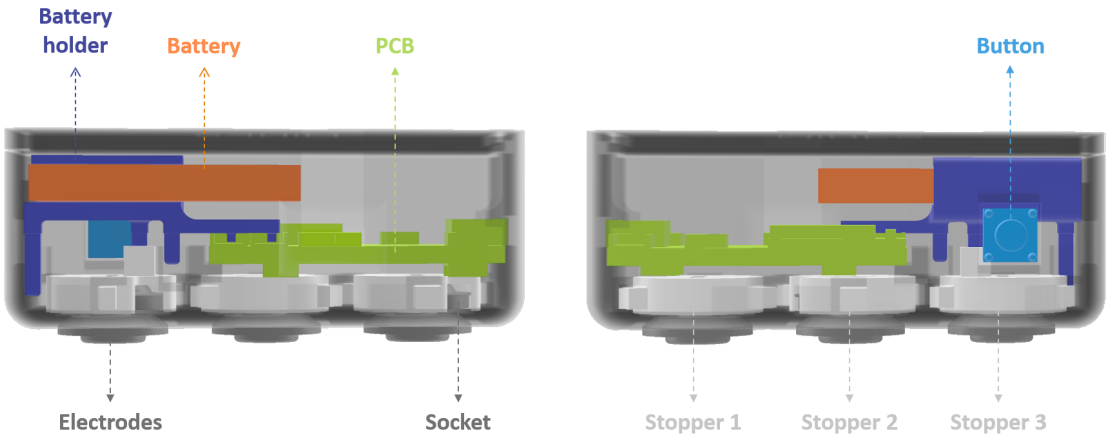

Figure 5.9: Components inside MYO box.

All the components inside the MYO box are fixed, as shown in Figure 5.9. Furthermore, the electrodes on the bottom surface result protrude; this design is due to a problem coming out from the first prints. At the beginning, the outing surface of electrodes was smaller, so when the box was fixed around the muscle of interest, some electrodes can not generate an optimal contact with the skin. An example is reported in Figure 5.10 where after sEMG acquisition of *Biceps Femoris*, a Notch filter at 50 Hz was applied via MATLAB.

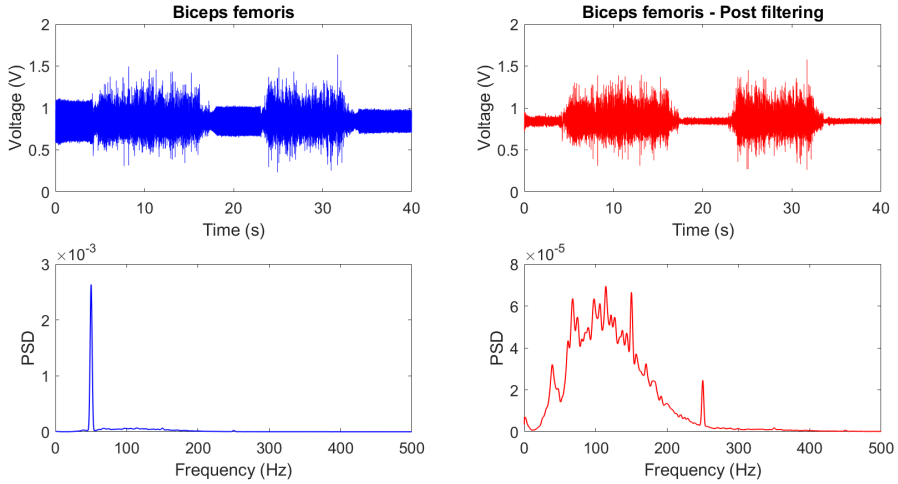

Figure 5.10: Notch filter via software.

Looking at the PSD, the network interference is evident in the blue signal, so the decision to augment the electrode's outing surface was taken to increase the contact area. The problem of contact can be understood because when the muscle contraction is done, that is visualized even in the blue signal where there is a lot of noise. The PSDs of signals have different y-axis; this is done because the network interference component is very high for the blue one.

Regarding the seven MYO boxes and the MYO support, all together, they represent the armband model. The armband was not printed but was only designed, and the final model is shown in the figure below. When the armband is closed, MYO boxes' position is the *CH1* - *CH7* positions defined for the 3DC model in section 5.1.

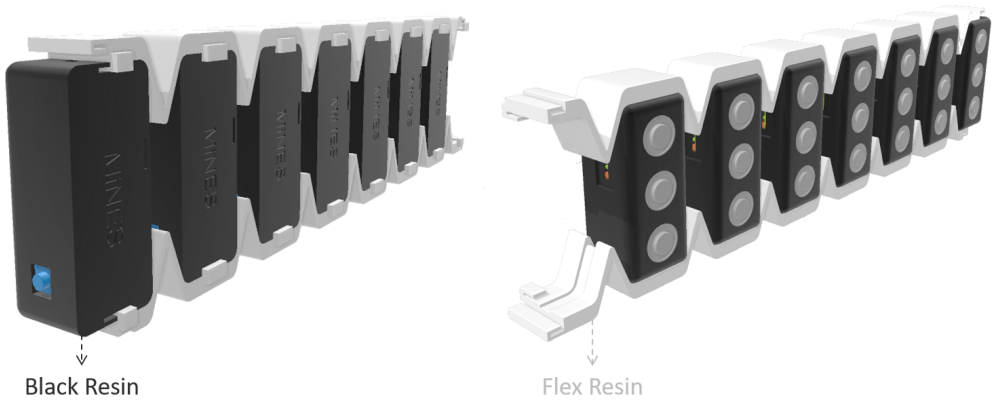

Figure 5.11: Myo model: rigid and flexible components.

Considering the possibility, for the moment, to use only one PCB, a single acquisition channel was tested. As shown in Figure 5.12, two side slots of 2 mm have been added to the model to fix it around the interested muscle. Inside that, there is the possibility to pass an elastic band.

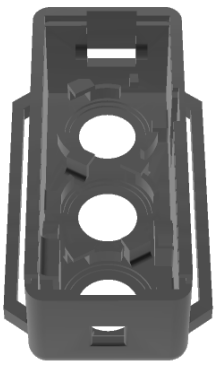

Figure 5.12: Myo box used for sEMG acquisition.

Chapter 6

MYO Box Acquisition

The final MYO box model, described in the previous chapter, was tested by acquiring other sEMG signals. With the aim to develop an electromyographic armband for gesture recognition, the last tests were done to evaluate PCB and channel acquisition box together. In this section, some sEMG signals were acquired using the improved PCB with all the MYO box components. As said before, to evaluate the quality of the sEMG signal, the SNR_{dB} of all muscle contractions was calculated considering the minimum value of acceptable quality equal to 10 dB. In this chapter, the acquisition was made in different configurations.
The first division concerns the limbs used:

- **Upper limbs**: movement performed were *wrist extension* and *forearm flexion*.
- **Lower limbs**: movement performed were *leg extension* and *leg flexion*.

Except for *wrist extension*, for all the other movements the contractions were standardize using different weights. For *wrist extension* were not use some weights but the Range Of Motion (ROM) was considered, as in section 4.3.1. Furthermore, for doing the same contraction, a point was fixed to a defined height. When the muscle was contracted, the extremity of the limb will reach the point in order to standardize the last one during the acquisitions.
The **weights** used are: *0 kg, 1 kg, 2 kg* and *4 kg*. Standardizing the acquisition with some weights, the idea is to see an increment of muscle contraction due to an increase of weight, looking at an augment of SNR_{dB}. For each movement with a different weight, 10 contractions of 10 seconds were done, separated each one of 30 seconds of resting phase. When the ten contractions were done, there is a resting phase of 2 minutes before the new weights acquisition. That was done to reduce muscle fatigue. Furthermore, 10 seconds of idle state was also acquired after every change of weights. To reduce the effect of muscle fatigue, the movements with the different weights are carried out in descending order, starting from 4kg and ending with 0kg.

For the evaluation of performance, the acquisition was made with two types of electrodes:

- **Wet electrode**, Mini adhesive disposable electrodes from COVIDIEN. They are characterized by a diameter equal to 24 mm, so to apply these to the MYO box, they were cut.
- **Dry electrode**, Non-gelled reusable Ag/AgCl by BITalino.

The acquisition with wet and dry allow comparing the calculated SNR_{dB}.
The acquisitions were made with the improved PCB and the data was not taken with the NI DAQ like before. The sEMG signal is directly transmitted from the PCB to the PC using the Bluetooth transmission of MCU. A Graphical User Interface (GUI) developed by the research group was used to connect the board with the computer. At the beginning, the ADC resolution of MCU was set to 14 bit and the sampling frequency was equal to 1000 Hz. With this configuration, there was a problem in Bluetooth packet transmission. Plotting ten seconds of sEMG acquisition data on GUI corresponded to thirty real seconds ones, so this is a problem for acquisition in real-time. Considering the sEMG signal band, the sampling frequency was reduced to 800 Hz (Nyquist theorem was respected considering the most information of sEMG signals is between 50-150 Hz) and the ADC resolution of MCU was set to 8 bit. Doing these changes, sEMG acquisition and transmission data were in real-time; in detail, the resulting time is equal to 25 ms for 20 bytes. Furthermore, the GUI permits to save the data in ".txt" format. These are imported and analyzed with some MATLAB scripts. The movements defined before was done with two different configurations of improved PCB:

- **PCB without DRL** circuit onboard;
- **PCB with DRL** circuit onboard.

The testing of PCB with and without the DRL circuit was done to increase the data for the analysis of the improvements introduced by DRL circuit implementation. Moreover, even if the project's final goal is to develop an armband evaluating the muscle activation of the forearm, sEMG signals of different muscles were acquired to test PCB and channel acquisition on different muscles and movements.

6.1 Upper Limbs

The upper limb can be separated into some parts. In particular, shoulder, arm, elbow, forearm, wrist, hand, and fingers compose it. The upper limb's parts can be moved all together or separately, depending on the movement that it wants to perform. In this case, two different movements are considered that include some muscle contractions. The MYO boxes were positioned on the top of the muscle interested for the execution of movements. In detail:

- **Extensor carpi radialis**, one of the most significant muscle used for doing *wrist extension*.
- **Biceps brachii**, muscle used for doing *forearm flexion*.

The muscles of the upper limbs are smaller and shorter than the lower limbs ones. They are less firmly attached to trunk so, they are characterized by high mobility. The sEMG signal acquisitions were made for the left arm. In Figure 6.1, an example of the application of MYO box was reported. In particular, the *biceps brachii* contraction with a weight of 4kg is shown.

Figure 6.1: Upper Limb: biceps brachii contraction with a weight of 4kg.

6.1.1 Wrist Extension

As said before, the Range Of Motion (ROM) was considered to standardize the wrist extension. For the idle state, the forearm is placed on a table, while the wrist extension was separated in three groups: *Minimal (0°-30°)*, *Normal (30°-60°)* and *Maximal (60°-90°)*.
Looking at the Figure 6.2, the expected behavior has been verified. In detail, with the increment of ROM, there is an increment in terms of muscle activation which is translated in an augment of SNR_{dB}. The SNR_{dB} augments considering the entire box and also considering the median value. That is verified for all the configurations, both for wet and dry electrodes both for No DRL and DRL circuit onboard.

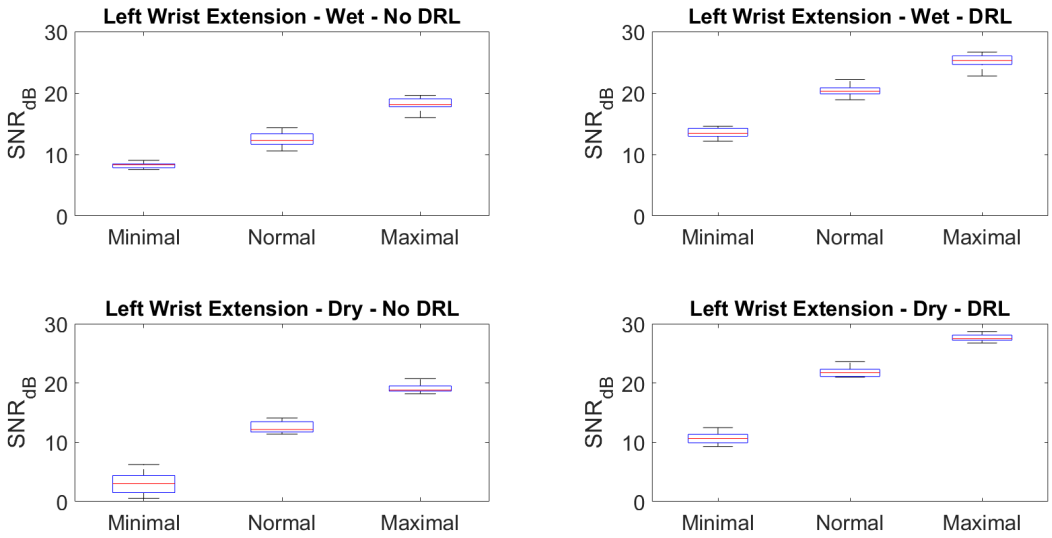

Figure 6.2: SNR_{dB} for extensor carpi radialis.

The boxplots contain the ten contractions did for each movement. The distribution of different contractions is very similar inside every box; that is done because the movement was standardized in order to have a similar muscle activation between each contraction. The height of the boxes is small and there aren't outliers. In addition to the information extracted from the boxplot, the mean value of ten contractions in different configurations has been calculated and the results are reported in Table 6.1. Making a comparison between the wet and dry electrodes, the SNR_{dB} values for wet ones are similar to the dry ones. We expected to have a higher value for wet electrodes, but sometimes dry ones seem to be greater. That may be due to a decrease in the adhesive effect of wet electrodes and, even if the muscle contraction is standardized, the effective muscle activation is not exactly the same considering the different contractions. Comparing the presence or not of the DRL circuit onboard, the highest SNR_{dB} was obtained with the PCB containing the DRL circuit both for wet and dry electrodes. Both for the two types of electrodes, only for minimal intensity without DRL on board the SNR_{dB} is smaller than 10 dB.

Table 6.1: SNR_{dB} for extensor carpi radialis. The values are expressed in dB.

		Wet electrodes		**Dry electrodes**	
Movement	Intensity	No DRL	DRL	No DRL	DRL
Wrist extension	minimal	8.22	13.46	3.06	10.74
	normal	12.42	20.38	12.51	21.85
	maximal	18.17	25.28	19.18	27.61

For all the other contractions, this value is higher than 10 dB, so the sEMG signal, acquired with different configurations, is good regarding the minimum value for evaluating sEMG signal quality. Considering the SNR_{dB} values for different movements, for wet electrodes, there is an average increment equal to ~6.8 dB, while for dry ones is equal to ~8.5 dB.
The effect of the DRL circuit onboard has been defined in terms of SNR_{dB} increment. Also, an analysis in terms of Power Spectral Density (PSD) was done. Considering the disadvantages introduced by the dry electrode and the first comparison between wet and dry ones in Figure 4.7, we aspect to have a significant component related to network interference and its harmonics. Looking at Figure 6.2, calculating the PSD of the signals, the noise component at 50 Hz and his harmonics aren't present. Before, it was used the NI DAQ to acquire and transmit data to a PC while now the data was transmitted to a PC using the Bluetooth antenna of MCU present on the PCB. The significant network interference is probably due to the data acquisition system and, before, the NI DAQ system introduced it.

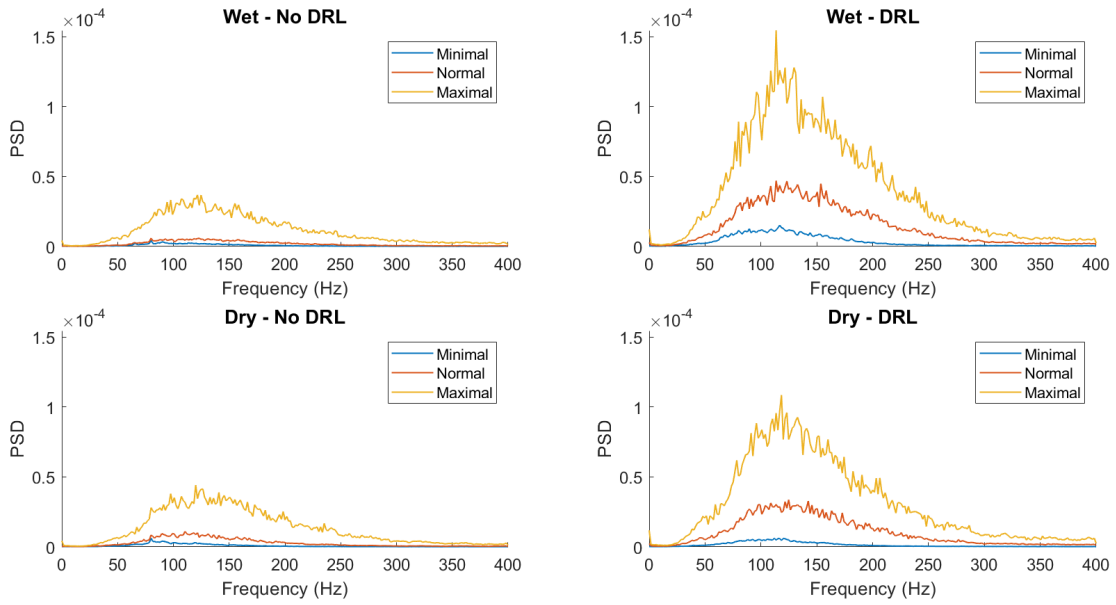

Figure 6.3: PSD for wrist extension.

Both for wet and dry electrodes, with the implementation of available DRL circuit onboard, an increment of PSD is verified. Considering the area under the curve, with the augmenting of muscle activation for doing different movements, there is an increment of PSD for all configurations. The area under the curve in the Power Spectral Density evaluation represents the signal's power, so there is a higher power with a higher curve. Making a comparison between the presence or not of the DRL circuit on PCB, there is an increment of the curve both for wet and dry electrodes

due to the presence of the DRL circuit. Making a comparison between wet and dry electrodes, the wet ones seem to have slightly greater PSD values. The DRL circuit application permits to have an increment both in terms of SNR_{dB} both in terms of PSD.

6.1.2 Forearm flexion

The use of four different weights (*0kg, 1kg, 2kg* and *4kg*) was applied to standardize the forearm flexion. For the idle state, the forearm is placed on a table, while for the execution of the movement, an isometric concentric contraction is performed. As shown in Figure 6.1, the same hand height was achieved with each weight in order to standardize the angle between the segments.
Considering all the acquisitions making in different configurations, the results obtained in terms of SNR_{dB} are reported in Figure 6.4. Looking at the boxplot, regarding all the configurations system, there is an increment of the SNR_{dB}. This incrementation is due to the augment of the weights with consequent increase in terms of muscle activation. The values present inside each box were the ten muscle contractions for each weight.

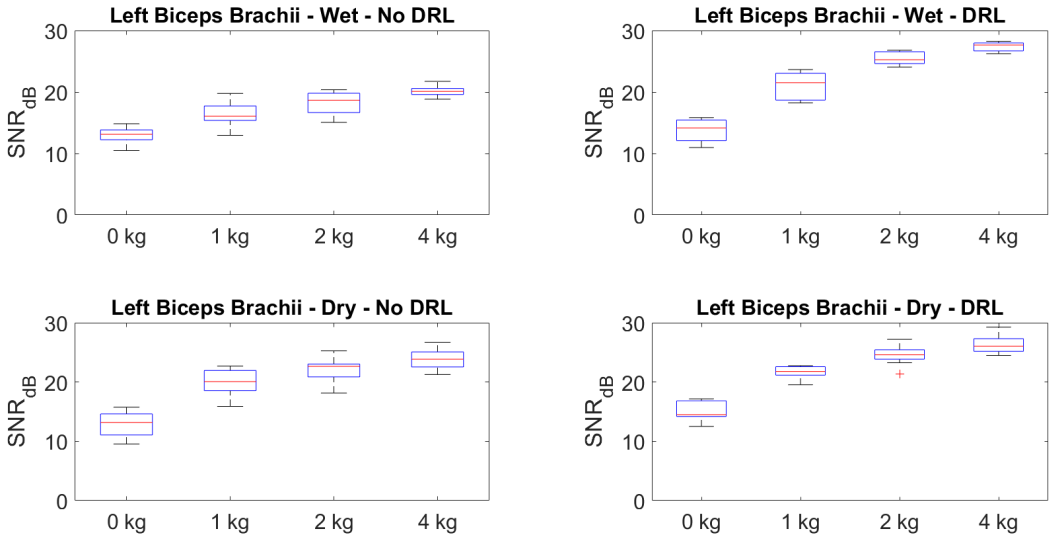

Figure 6.4: SNR_{dB} for biceps brachii.

Looking at the boxes' heights representing the distribution of SNR_{dB}, the data seem to be characterized by low variability. There is only one outlier in a contraction with a weight of 2 kg, using the configuration system characterized by the dry electrodes and DRL circuit on PCB. This outlier is due to a small distribution of muscle contraction during the movement performed. In particular, the 25th Percentile is

equal to 23.85 dB, the 75th Percentile is equal to 25.44 dB, so the minimum value acceptable to not fix an outlier is 21.47 dB. The resulting outliers value is equal to 21.41 dB, so it is very close to the lower limit. It results an outlier due to the calculation of boxplot, but at the same time, the value is good in terms of SNR_{dB} because it is greater than the minimum value of acceptable sEMG signal quality. Furthermore, there is only one SNR_{dB} lower than 10 dB for a muscle contraction with 0 kg, using dry electrodes and PCB without DRL. In this case, the SNR_{dB} is equal to 9.54 dB.
With the increase of muscular effort, the SNR_{dB} augment also considering the median value. Comparing the DRL circuit's evaluation, the highest SNR_{dB} were obtained using the PCB containing the DRL circuit, both for wet and dry electrodes.
Besides, the mediated SNR_{dB} values on all configurations were calculated and reported in Table 6.2. Also this time, comparing wet and dry electrodes, the SNR_{dB} value are similar; sometimes dry ones are higher than wet ones. The behavior is respected; with the increase of weight, the SNR_{dB} increase.

Table 6.2: SNR_{dB} for brachial bicep. The values are expressed in dB.

		Wet electrodes		**Dry electrodes**	
Movement	Weight	No DRL	DRL	No DRL	DRL
Forearm flexion	0 kg	12.98	13.73	12.89	15.08
	1 kg	16.26	21.17	19.73	21.70
	2 kg	18.16	25.38	22.05	24.52
	4 kg	20.12	27.41	23.95	26.42

For the DRL circuit evaluation, making a comparison between the PCB with and without DRL, both for wet and dry electrodes, the highest values were obtained for the PCB containing the DRL onboard. The average increment for wet electrode is equal to ~5.04 dB while for dry electrode is ~2.28 dB. Considering the acceptable value for good sEMG signal quality, the SNR_{dB} calculated are characterized by high values.
Considering the contraction without weights, the average SNR_{dB} is higher than 10 dB for all the configurations. Augmenting the weights, as expected, the parameter increase. With the maximum weights of 4 kg, SNR_{dB} higher than 20 dB was obtained for all the configurations, so good quality for muscle activation detection.

6.2 Lower Limbs

The lower limb can be separated into hip, leg, knee, leg, ankle, foot and toes. Also this time, the different parts can be moved together or separately; generally,

the upper limbs' movements are finer than the lower ones. Two movements are considered for the test and the muscles surrounded by MYO box are:

- **Vastus lateralis**, one of the most significant muscle used for doing *leg extension*.
- **Biceps femoris**, muscle used for doing *leg flexion*.

The muscles of the lower limbs are larger and longer than the upper limbs ones. They are more firmly attached to the trunk so, they are characterized by low mobility. The sEMG signal acquisitions were made for the right leg. In particular, the *biceps femoris* contraction with a weight of 4kg is shown in Figure 6.5.

Figure 6.5: Upper Limb: biceps femoris contraction with a weight of 4kg.

6.2.1 Leg extension

The use of four different weights (*0kg, 1kg, 2kg* and *4kg*) was applied to standardize the leg extension. The idle state is represented by the person sitting on a physiotherapy bed with the legs dangling. In addition to weights, to standardize muscle contraction during leg extension, the foot's dorsum reached the same height in order to don't hyperextend the leg with a lower weight.
For all the contraction the SNR_{dB} was calculated and the values obtained are shown in Figure 6.6. Looking the boxplots, the behavior is respected. Inside each box there are ten contractions and with the increment of weights there is an increment of SNR_{dB}. The increment is less evident than the results obtained for upper limbs, that can be due to the structure of lower limbs muscle.
Considering all the configurations, the median values increase with the augmenting of muscle activation and all the boxes are characterized by small height. There are four outliers due to the small distribution of SNR_{dB} values. The worst-case there is considering the weight of 1 kg with the wet electrode and DRL circuit. The 25th Percentile is equal to 17.26 dB, the 75th Percentile is equal to 18.21 dB, so the minimum value to don't have an outlier is equal to 15.84 dB. The anomalous value is equal to 15.47 dB, so the difference between the limit and the value is small in

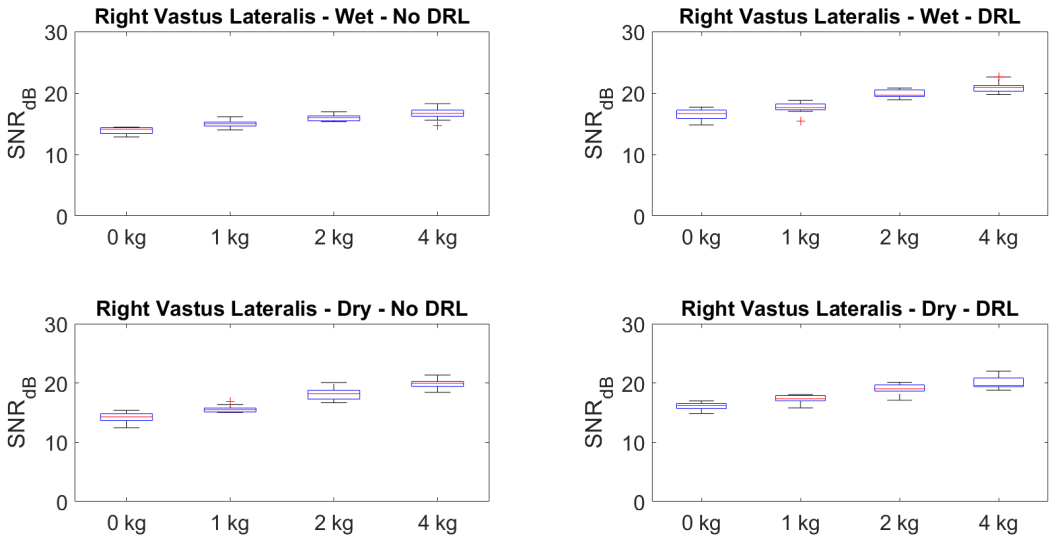

Figure 6.6: SNR_{dB} for vastus lateralis.

the worst case. The generation of this anomalous value is due to the calculation of boxplot, but considering SNR_{dB}, the value is higher than the fixed limit of 10 dB. Looking at the distribution, the muscle activation of vastus lateralis for doing leg extension is characterized by SNR_{dB} values higher than 10 dB for all the contractions. Comparing the presence or not of DRL circuit on PCB, the SNR_{dB} seems to be higher for the DRL one respect the other one.
The average SNR_{dB} are grouped in Table 6.3. Making a comparison between electrodes, the wet ones were characterized by higher values than dry ones for the PCB with DRL circuit on board while the wet ones combined with PCB without the DRL have lower SNR_{dB} than dry ones.

Table 6.3: SNR_{dB} for vastus lateralis. The values are expressed in dB.

		Wet electrodes		**Dry electrodes**	
Movement	Weight	No DRL	DRL	No DRL	DRL
Leg extension	0 kg	13.86	16.45	14.17	16.12
	1 kg	15.02	17.56	15.64	17.29
	2 kg	15.99	19.85	18.18	18.90
	4 kg	16.59	21.04	19.87	20.01

Considering the electrodes separately, the DRL circuit permits to have higher values than PCB without DRL both for wet and dry electrodes. The average increment

due to the DRL circuit is equal to ~3.36 dB for wet electrodes and to ~1.12 dB for dry electrodes. Regarding the different weights, the SNR_{dB} are characterized by higher values than 10 dB, so the quality of sEMG signal acquired with improved PCB and MYO box is good to acquire contractions of vastus lateralis.

6.2.2 Leg flexion

To standardize leg flexion four different weights (*0kg, 1kg, 2kg* and *4kg*) were used. As shown in Figure 6.5, in addition to weights for standardize muscle activation during leg flexion, the heel reached the same height during all the movements' execution. The person in the standing position represents the idle state.
Looking at Figure 6.7, all the SNR_{dB} are reported and inside a box, there are the ten contractions performed for each configuration. Also considering leg flexion, the behavior expected was respected. With the augment of weight, it is possible to see an augment of SNR_{dB} calculated less evident than upper limbs.

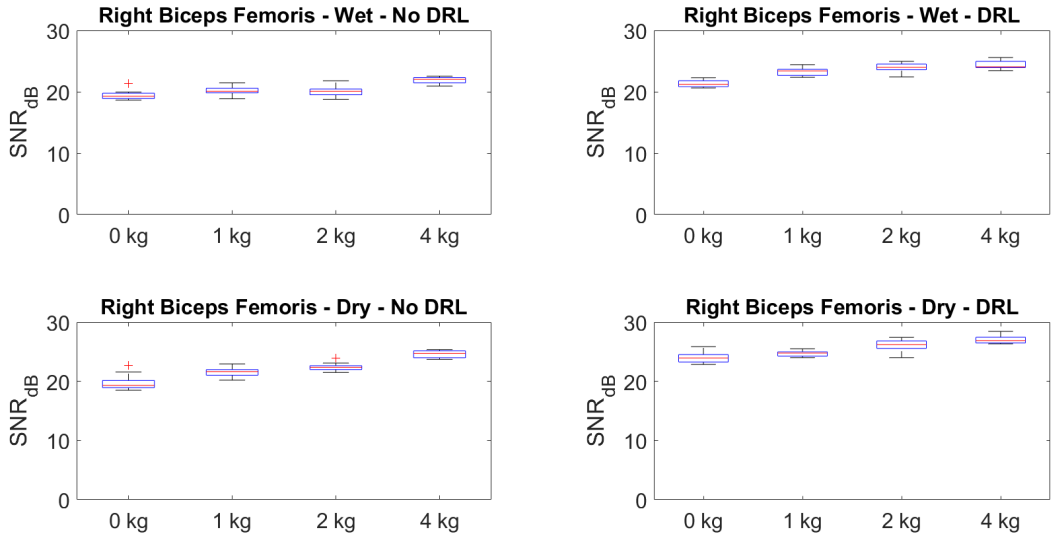

Figure 6.7: SNR_{dB} for biceps femoris.

As shown in Figure 6.7, the values seem to be higher than ~20 dB even in the worst case of 0 kg, which means with this movement, the sEMG acquisition is characterized by good signal quality greater than 10 dB. The median value increases with the augment of weights and the boxes result in a small height. A small distribution characterizes the values calculated for each contraction, the movement result to be standardized. Considering all boxes, there are only three outliers. The worst case is for a weight of 0kg with wet electrodes and PCB without DRL circuit configuration. The SNR_{dB} dB values are equal to 18.90 dB for 25th Percentile,

19.77 dB for 75th Percentile and the upper limit to define an outlier is equal to 21.08 dB. The anomalous value is equal to 21.36 dB. The outlier results to be an anomalous value due to the boxplot's calculation, but this is because the movement is well standardized and the distribution is small. The difference of its SNR_{dB} value than the limits is small and higher than the signal quality limit.
In Table 6.4, the average SNR_{dB} mediated between the ten contractions is reported. Dry electrodes seem to have a higher value than wet ones. Probably that is due to a better fixation of MYO box with the elastic band than the fixation of the wet ones where the MYO box is attached to the skin only thanks to the adhesive part of the wet electrode. The SNR_{dB} is very high; in the worst situation with a weight of 0 kg and without DRL circuit on PCB, the value is higher than 19 dB; in all the other situation, it is higher than 20 dB. Only for wet and dry electrodes, the implementation of DRL circuit permits an increment for all the weights. In particular, there is an average increment equal to ~2.87 dB for wet ones and equal to ~3.41 dB for dry ones.

Table 6.4: SNR_{dB} for bicep femoris. The values are expressed in dB.

		Wet electrodes		**Dry electrodes**	
Movement	Weight	No DRL	DRL	No DRL	DRL
Leg flexion	0 kg	19.46	21.30	19.80	24.10
	1 kg	20.12	23.30	21.56	24.71
	2 kg	20.07	23.97	22.45	26.12
	4 kg	21.85	24.39	24.59	27.09

Considering all the results obtained with upper and lower limbs, the DRL circuit application on PCB permits to have an increment in terms of Signal-to-Noise Ratio (dB) and, in the frequency domain, an increment of Power Spectral Density. These results were verified for all the acquisitions standardize with weights or ROM, both for wet and dry electrodes. For making these acquisitions, two MYO boxes containing the PCB with DRL and the other containing the PCB without DRL circuit were used. 6 dry electrodes (three for each box) and 24 wet electrodes (three for every different movement) were used to acquire all the movements. The advantage of dry ones is the reusability; so, it is possible to use a single configuration to acquire signals from different muscles. In contrast, with wet ones, it is necessary to change electrodes when changing the muscle acquired. The use of dry electrodes is fundamental in order to develop an electromyographic armband for doing gesture recognition and with these results, the signal quality seems to be good.

6.3 Towards an armband

Using the MYO box was done the same acquisition defined in Section 4.2 in order to simulate the sEMG signal acquired for hand gesture recognition. Considering the results obtained in Section 6.1 and 6.2, the PCB with DRL circuit on board was inserted inside the MYO box and dry electrodes were applied. This configuration represents the acquisition system. As in Section 4.2, the acquisition system was positioned on the top of the interested muscle. When the sequence of movement was done, the MYO box was positioned on the top of another muscle. The MYO box positions are the *CH1-CH7* defined in Section 5.1.
In Figure 6.8 are reported the sEMG signals and the ATC signals extracted as defined in Section 4.2.2; in detail, the blue one represents the sEMG while the orange one represents the ATC. On the y axis, the MYO box position is specified, but there isn't the measuring unit. That is done to overlap the ATC and sEMG signals, the value is normalized respect the maximum due to different magnitude orders. Looking at the figure, the ATC signals seems to follow the sEMG trend.

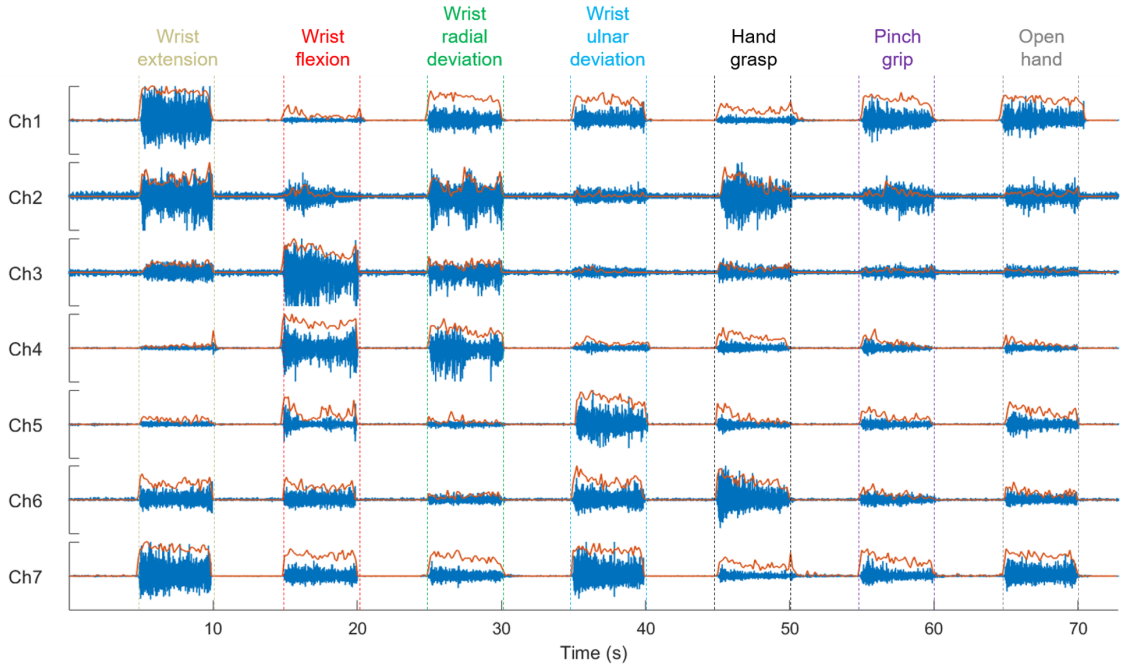

Figure 6.8: Gesture recognition.

Considering all the movements performed and the MYO box's different positions, the SNR_{dB} was calculated and the results are reported in Table 6.5. As before, the small values represent a small activation of the muscle acquired for doing a specific movement but comparing the results obtained with the previous acquisition system and reported in Table 4.3, this time all the SNR_{dB} are higher than 0 dB. Having

only positive values means the system can detect also a small muscle activation with respect to the noise signal.
For example, taking *"Wrist Extension"*, the highest value are obtained for *"CH1"* and *"CH7"* and that are greater than ~25 dB. *"CH1"* and *"CH7"* represent the muscles mostly activated for doing wrist extension.

Table 6.5: SNR_{dB} of forearm muscles. The values are expressed in dB.

Channel	**Extension**	**Flexion**	**Radial**	**Ulnar**	**Grasp**	**Grip**	**Open**
Ch1	25.94	4.04	18.13	16.83	8.29	19.34	19.75
Ch2	12.92	5.54	11.92	2.52	13.19	8.30	6.28
Ch3	7.45	16.19	8.83	1.32	4.89	2.61	0.41
Ch4	6.51	21.02	23.11	10.01	12.51	10.57	8.28
Ch5	5.84	10.08	6.04	20.10	9.28	9.50	12.92
Ch6	14.37	13.41	8.10	16.18	18.67	9.34	10.02
Ch7	25.89	18.52	16.55	25.01	12.36	16.28	21.07

An average of SNR_{dB} considering the different movements performed and acquired with the seven MYO boxes are reported below. Doing this average the SNR_{dB} will decrease because it was considered all the muscles for each movement but for doing a specific movement, certain muscles are activated while others not.
The average SNR_{dB} obtained is higher than 10 dB. Even if for the calculation of this value muscles activated and not are considered, the parameter gives good information in terms of signal quality for each movement performed. That is important because the signal's quality is fundamental for calculating ATC signals and, subsequently, for doing gesture recognition. Considering the different movements, the SNR_{dB} values were equal to:

Movement	**SNR_{dB}**
Wrist extenson	14.13 dB
Wrist flexion	12.69 dB
Wrist radial deviation	13.24 dB
Wrist ulnar deviation	13.14 dB
Hand grasp	11.31 dB
Pinch grip	10.85 dB
Open hand	11.25 dB

Finally, the average SNR_{dB} separated for the acquisition channel was calculated and reported below. These values give the information of muscle activation during the execution of the 7 movements performed. For example, *CH3*, which represents the *extensor carpi ulnaris*, has the lowest value that means it is the muscle less activated for doing the sequence of movement. Otherwise, *CH7*, which represents the *brachioradialis*, has the highest value and it represents the most activated muscle. Considering the different channel position, the SNR_{dB} values were equal to:

Channel	**SNR_{dB}**
CH1	16.05 dB
CH2	8.67 dB
CH3	5.96 dB
CH4	13.14 dB
CH5	10.54 dB
CH6	12.87 dB
CH7	19.38 dB

Chapter 7

Conclusion and Future works

This thesis proposed an analysis of sEMG signal quality in terms of SNR_{dB}. In order to develop an electromyographic armband for hand gesture recognition, to acquire the signal dry electrodes were used and some PCBs developed by the research group. The final goal is to develop an embedded low-power system based on the Average Threshold Crossing (ATC) technique.

In the first part, different upper limbs movements were performed and acquired with a Data Acquisition System (DAQ) to test three different dry electrodes: BiosignalPlux Conductive Lycra by MindtecStore, Non-gelled Reusable Ag / AgCl with velcro by BITalino and Non-gelled Reusable Ag / AgCl by BITalino. The third one was chosen and used for all the next acquisitions because it is the best trade-off between SNR_{dB} and costs.

Once choose the electrodes, in order to increase the sEMG signal quality it was tested the application of Driven-Right-Leg (DRL) circuit available on board. Different movements of upper limbs were performed and with the PCB containing DRL, the highest value of SNR was obtained. The minimum value to define a sEMG signal of good quality was set to 10 dB, the average SNR_{dB} was equal to ~8.13 dB for PCB without DRL and ~11.71 dB for PCB containing DRL. Furthermore, considering the frequency domain, thanks to the application of DRL, the Power Spectral Density (PSD) of the signals improves.

Subsequently, two 3D models of an armband for hand gesture recognition were designed: 3D model and MYO model, each characterized by 7 acquisition channels. An improved PCB characterized by the MicroController Unit (MCU) presence onboard with all the other components necessary to insert inside the box represented

the starting point to develop the wearable device model. One package of the MYO model was effectively prototyped to perform the tests.

In the last part of the thesis, the printed acquisition channels and the improved PCB were tested in different configurations for the upper and lower limbs. In order to increase the SNR_{dB}, the Bluetooth antenna present on MCU is used to transmit data and reduce noise introduced by DAQ system. Considering all the acquisition, the SNR_{dB} obtained for PCB containing DRL is higher than PCB without DRL. In detail, the first one is equal to ~21.15 dB while the second one is equal to ~16.98 dB. The results obtained with dry electrodes and PCB containing DRL demonstrate a good quality in terms of SNR_{dB}; so, with this configuration is possible to make sEMG signal acquisition. Subsequently, this can be used to extract ATC signals and doing gesture recognition.

There are several possible developments concerning this thesis work. From the hardware point of view, it can be possible to print the flexible part of the MYO model and the seven acquisition boxes in order to test the designed model. That is necessary to have an user-friendly armband and easy to place on the forearm. It is also possible to improve some parts of the PCB. For example, considering the socket to connect the electrode. At the moment, the sockets are connected to the PCB with some wires; an improvement can be to fix the sockets directly on board to decrease the possibility of having movement artifacts during dinamic acquisitions.

Once the 3D model is tested, next step could be to acquire the sEMG signals from the different forearm muscles in order to generate a dataset for hand gesture recognition. In a first analysis, the sEMG signal can be acquired with the MYO model and the extraction of the ATC signal can be made via software for training and testing the machine learning algorithm. Once tested offline, it can be possible to directly charge the classifier on the MCU present on the PCB and evaluate the classification in real-time directly onboard.

Bibliography

[1] Shane W. Cummings and Christopher Tangen. *Human muscle system*. URL: https://www.britannica.com/science/human-muscle-system.

[2] URL: https://www.teachpe.com/anatomy-physiology/types-of-muscle.

[3] Biga et al. *10.2 Skeletal Muscle*. URL: https://open.oregonstate.education/aandp/chapter/10-2-skeletal-muscle/.

[4] Neuro Doc Gnanapavan. Mar. 2015. URL: https://multiple-sclerosis-research.org/2015/03/mitochondria-again-but-this-time-in-muscle/.

[5] Cindy L. Stanfield. *Fisiologia del muscolo*. EdiSES s.r.l. - Napoli, 2012. Chap. 12, pp. 322–359. ISBN: 9788879597142.

[6] URL: https://www.pinterest.it/pin/732538695620774584/.

[7] iandanforth. *Motor Unit*. Feb. 2019. URL: https://github.com/iandanforth/pymuscle.

[8] URL: https://www.teachpe.com/anatomy-physiology/shapes-of-skeletal-muscle.

[9] URL: https://courses.lumenlearning.com/boundless-ap/chapter/overview-of-the-muscular-system/.

[10] *Anterior Forearm*. June 2016. URL: https://basicmedicalkey.com/anterior-forearm/.

[11] *Forearm Muscles: Origin, Insertion, Nerve Supply Action*. URL: https://www.howtorelief.com/forearm-muscles-origin-insertion-nerve-supply-action/.

[12] *Posterior Forearm*. June 2016. URL: https://basicmedicalkey.com/posterior-forearm/.

[13] *Action potential velocity*. URL: https://www.khanacademy.org/test-prep/mcat/organ-systems/neuron-membrane-potentials/a/action-potential-velocity.

[14] Luca Mesin. *BIOELECTRIC SIGNALS*. Luca Mesin, 2017. Chap. 8, pp. 245–253. ISBN: 9788892332485.

[15] Scott Freeman; Healy Hamilton. 2nd ed. 2005.

[16] Cindy L. Stanfield. *Cellule nervose e segnali elettrici*. EdiSES s.r.l. - Napoli, 2012. Chap. 7, pp. 166–195. ISBN: 9788879597142.

[17] Dario Farina Roberto Merletti. "Analysis of intramuscular electromyogram signals". In: *The Royal Society* (Nov. 2008), pp. 357–368. DOI: 10.1098/rsta.2008.0235.

[18] Andrew D. Vigotsky et al. "Interpreting Signal Amplitudes in Surface Electromyography Studies in Sport and Rehabilitation Sciences". In: *Frontiers in Physiology* (Jan. 2018). DOI: 10.3389/fphys.2017.00985.

[19] Muhammad Zahak Jamal. *Signal Acquisition Using Surface EMG and Circuit Design Considerations for Robotic Prosthesis*. Ganesh R. Naik, Oct. 2012. DOI: http://dx.doi.org/10.5772/52463.

[20] Alexander Adam et al. Carlo J. De Luca. "Decomposition of Surface EMG Signals". In: *The American Physiological Society* (May 2006), pp. 1646–1657. DOI: 10.1152/jn.00009.2006.

[21] Runer Augusto Marson César Ferreira Amorim. *Application of Surface Electromyography in the Dynamics of Human Movement*. Ganesh R. Naik, Oct. 2012. Chap. 16. DOI: http://dx.doi.org/10.5772/52463.

[22] Carlo J. De Luca. "Surface Electromyography: Detection and Recording". In: *DelSys Incorporated* (2002).

[23] Dr. Scott Day. "Important Factors in Surface EMG Measurement". In: *Bortec Biomedical Ltd* ().

[24] S. Tam et al. M. Roudjane. "Detection of Neuromuscular Activity Using New Non-Invasive and Flexible Multimaterial Fiber Dry-Electrodes". In: *IEEE* (2019). DOI: http://dx.doi.org/10.1109/JSEN.2019.2933751.

[25] *Mini Adhesive Electrodes*. URL: https://shop.neurospec.com/mini-adhesive-electrodes-covidien.

[26] *Non-gelled Reusable Ag/AgCl*. URL: https://plux.info/electrodes/60-non-gelled-reusable-agagcl-electrodes.html.

[27] Peyman Fayyvaz Shahandashti et al. "Highly conformable stretchable dry electrodes based on inexpensive flex substrate for long-term biopotential (EMG /ECG) monitoring". In: *Sensors and Actuators A: Physical* (June 2019). DOI: https://doi.org/10.1016/j.sna.2019.06.041.

[28] Christopher Spiewak et al. "A Comprehensive Study on EMG Feature Extraction and Classifiers". In: *Lupine Publishers* (Feb. 2018). DOI: 10.32474/OAJBEB.2018.01.000104.

[29] B. Sereni. "Design and development of a low-power wearable device for the acquisition of surface electromyography (sEMG) signals with average threshold crossing (ATC)". 2016.

[30] F. Rossi. "Low Power System for Event-Driven Control of Functional Electrical Stimulation". 2017.

[31] A. Mongardi. "A Low-Power Embedded System for Real-Time EMG based Event-Driven Gesture Recognition". 2019.

[32] *What is Machine Learning: Supervised, Unsupervised, Semi-Supervised and Reinforcement learning methods*. June 2020. URL: https://towardsdatascience.com/what-is-machine-learning-a-short-note-on-supervised-unsupervised-semi-supervised-and-aed1573ae9bb.

[33] Rudolph Russel. *Machine Learning*. 2018. Chap. 1.

[34] *Getting started with Machine Learning*. May 2020. URL: https://www.geeksforgeeks.org/getting-started-machine-learning/?ref=lbp.

[35] Liu Xumin et al. Shi Na. "Research on k-means Clustering Algorithm. An Improved k-means Clustering Algorithm". In: *IEEE Computer Society, Third International Symposium on Intelligent Information Technology and Security Informatics* (2010). DOI: 10.1109/IITSI.2010.74.

[36] F. Pedregosa et al. "Scikit-learn: Machine Learning in Python". In: *Journal of Machine Learning Research* 12 (2011), pp. 2825–2830.

[37] Ayon Dey. "Machine Learning Algorithms: A Review". In: *International Journal of Computer Science and Information Technologies* (2016).

[38] *Decision Tree Classification Algorithm*. URL: https://www.javatpoint.com/machine-learning-decision-tree-classification-algorithm.

[39] William S Noble. "What is a support vector machine?" In: *Nature Publishing Group* (Dec. 2006).

[40] *Maximum margin classification with support vector machines*. URL: https://subscription.packtpub.com/book/big_data_and_business_intelligence/9781783555130/3/ch03lvl1sec21/maximum-margin-classification-with-support-vector-machines.

[41] *Support Vector Machines with the mlr package*. Oct. 2019. URL: https://www.r-bloggers.com/2019/10/support-vector-machines-with-the-mlr-package/.

[42] Dec. 2014. URL: https://themasterpiece1.wordpress.com/2014/12/01/666-and-the-thinking-computerto-be-updated-proof-will-be-added/.

[43] Marco Crepaldi et al. “A quasi-digital radio system for muscle force transmission based on event-driven IR-UWB”. In: *IEEE Biomedical Circuits and Systems Conference (BioCAS)* (2012), pp. 116–119.

[44] Paolo Motto Ros et al. “A wireless address-event representation system for ATC-based multi-channel force wireless transmission”. In: *5th IEEE Internatinal Workshop on Advances in Sensors and Iterfaces IWASI* (2013), pp. 51–56.

[45] Danilo Demarchi et al. “Low-Power long term sEMG monitoring modular system”. 2019.

[46] D. A. F. Guzman et al. “Very low power event-based suface EMG acquisition system with off-the-shelf components”. In: *IEEE Biomedical Circuits and Systems Conference (BioCAS)* (2017), pp. 1–4. DOI: 10.1109/BIOCAS.2017.8325152.

[47] Stefano Sapienza et al. “On-Line Event-Driven Hand Gesture Recognition Based on Surface Electromyographic Signals”. In: *IEEE International Symposium on Circuits and Systems (ISCAS)* (May 2018), pp. 1–5. DOI: 10.1109/ICECS46596.2019.8964944.

[48] Vincenzo Barresi. “Machine Learning Approaches for Embedded Real-Time Gesture Recognition”. July 2020.

[49] Matteo Tolomei. “Towards an Electromyographic Armband: an Embedded Machine Learning Algorithms Comparison”. Dec. 2020.

[50] Rafiqul Zaman Khan and Noor Adnan Ibraheem. “Hand Gesture Recognition: a literature review”. In: *International journal of Artificial Intelligence Applications* (July 2012). DOI: 10.5121/ijaia.2012.3412.

[51] Munir Oudah et al. “Hand Gesture Recognition Based on Computer Vision: A review of Techniques”. In: *Journal of Imaging* (July 2020). DOI: 10.3390/jimaging6080073.

[52] Peide Zhu et al. “Control with Gestures: A Hand Gesture Recognition System Using Off-the-Shelf Smartwatch”. In: *IEEE 2018 4th International Conference on Big Data Computing and Communications* (2018). DOI: 10.1109/BIGCOM.2018.00018.

[53] Khanh Nguyen Trong et al. “Recognizing Hand Gestures for Controlling Home Appliances with Mobile Sensors”. In: *IEEE Conference Paper* (Sept. 2019). DOI: 10.1109/KSE.2019.8919419.

[54] Biao MA et al. “A Robot Control System Based on Gesture Recognition Using Kinect”. In: *Telkomnika* (May 2013).

[55] Siddharth S. Rautaray and Anupam Agrawal. “Interaction with Virtual Game through Hand Gesture Recognition”. In: *IEEE* (2011).

[56] Ming Jin Cheok et al. "A review of hand gesture and sign language recognition techniques". In: *Springer-Verlag GmbH Germany* (Aug. 2017). DOI: 10.1007/s13042-017-0705-5.

[57] Juan P. Wachs et al. "A Gesture-based Tool for Sterile Broesing of Radiology Images". In: *Journal of the American Medical Informatics Association* (June 2018). DOI: 10.1197/jamia.M241.

[58] Mohidul Alam Laskar et al. "Stereo Vision-based Hand Gesture Recognition under eD Environment". In: *ScienceDirect* (2015). DOI: 0.1016/j.procs.2015.08.053.

[59] Nicolò Bargellesi et al. "A Random Forest-based Approach for Hand Gesture Recognition with Wireless Wearable Motion Capture Sensors". In: *IFAC PapersOnLine* (2019). DOI: 10.1016/j.ifacol.2019.09.129.

[60] Tushar Chouhan et al. "Smart Glove with Gesture Recognition Ability For The Hearing And Speech Impaired". In: *IEEE* (Sept. 2014). DOI: 978-1-4799-4097-4/14.

[61] Simone Benatti et al. "A Versatile Embedded Platform for EMG ACquisition and Gesture Recognition". In: *IEEE* (Oct. 2015). DOI: 10.1109/TBCAS.2015.2476555.

[62] Weidong Geng et al. "Gesture recognition by istantaneous surface EMG images". In: *Nature Scientific Report* (Nov. 2016). DOI: 10.1038/srep36571.

[63] *gForcePro EMG Armband*. URL: https://www.teachpe.com/anatomy-physiology/types-of-muscle.

[64] Paolo Visconti et al. "Technical Features and Functionalities of Myo Armband: An overview on Related Literature and Advanced Applications of Myoelectric Armbands Mainly Focused on Arm Prostheses". In: *International journal smart sensing and intelligent systemst* (Feb. 2018). DOI: 10.21307/ijssis-2018-005.

[65] Ulysse Coté-Allard et al. "A Low-Cost, Wireless, 3-D-Printed Custom Armband for sEMG Hand Gesture Recognition". In: *Sensors* (June 2019). DOI: 10.3390/s19122811.

[66] Ali Moin et al. "A wearable biosensing system with in-sensor adaptive machine learning for hand gesture recognition". In: *Nature electronics* (Oct. 2020). DOI: 10.1038/s41928-020-00510-8.

[67] A. Melaku, Dinesh Kumar, and A. Bradley. "Influence of inter-electrode distance on EMG". In: vol. 2. Feb. 2001, 1082–1085 vol.2. ISBN: 0-7803-7211-5. DOI: 10.1109/IEMBS.2001.1020377.